PREFORMULATION OF TOPICAL CHEMOPREVENTIVE AGENTS AND THE SOLUBILITY ESTIMATION OF HYDRATED SOLUTES

by

Stephen J. Franklin

_____

A Dissertation Submitted to the Faculty of the

DEPARTMENT OF PHARMACEUTICAL SCIENCE

In Partial Fulfillment of the Requirements

For the Degree of

DOCTOR OF PHILOSOPHY

In the Graduate College

THE UNIVERSITY OF ARIZONA

2015

GRADUATE COLLEGE

As members of the Dissertation Committee, we certify that we have read the dissertation prepared by Stephen J Franklin, titled "Preformulation of Topical Chemopreventive Agents and the Solubility Estimation of Hydrated Solutes" and recommend that it be accepted as fulfilling the dissertation requirement for the Degree of Doctor of Philosophy.

_____ Date: (5 December 2014)
Dr. Paul B. Myrdal

_____ Date: (5 December 2014)
Dr. Samuel H. Yalkowsky

_____ Date: (5 December 2014)
Dr. Michael Mayersohn

_____ Date: (5 December 2014)
Dr. Heidi Mansour

Final approval and acceptance of this dissertation is contingent upon the candidate's submission of the final copies of the dissertation to the Graduate College.

I hereby certify that I have read this dissertation prepared under my direction and recommend that it be accepted as fulfilling the dissertation requirement.

_____ Date: (5 December 2014)
Dissertation Director: Dr. Paul B. Myrdal

STATEMENT BY AUTHOR

This dissertation has been submitted in partial fulfillment of the requirements for an advanced degree at the University of Arizona and is deposited in the University Library to be made available to borrowers under rules of the Library.

Brief quotations from this dissertation are allowable without special permission, provided that an accurate acknowledgement of the source is made. Requests for permission for extended quotation from or reproduction of this manuscript in whole or in part may be granted by the head of the major department or the Dean of the Graduate College when in his or her judgment the proposed use of the material is in the interests of scholarship. In all other instances, however, permission must be obtained from the author.

SIGNED: Stephen J. Franklin

ACKNOWLEDGMENTS

Your dreams are not often achieved alone. They are a (long!) journey with the people who love you the most. I have been very fortunate to have so many loyal and loving friends and family members who have been with me every step of the way. First off, I would like to thank my amazing wife for all your love, support, and encouragement during this journey. I would not be here without you. I would like to thank my advisor Dr. Paul Myrdal for his guidance over the past few years. Your enthusiasm and expertise has been instrumental to my growth as a scientist and your friendship has been even more valuable to me as a person.

I would like to thank my graduate committee, Dr. Samuel Yalkowsky, Dr. Michael Mayersohn, and Dr. Heidi Mansour. You all have been instrumental to my scientific development and I am thankful for your influence. A special thank you to all my colleagues and friends throughout the years at the University of Arizona. It has been a privilege to spend this time with you all.

To all my friends and family I say thank you. It's difficult to name you all but a few must be mentioned. To my grandparents Judy and Andy Andrews. Thank you for kick starting my scientific curiosity and more importantly for your unconditional love. To my great friend Jared Romero. Thank you for always picking me up when I am down and for never letting me doubt myself, ever. Finally to Clover, thank you for making our family whole.

DEDICATION

To my best friend, biggest supporter and greatest love. To my wife, Sheena.

TABLE OF CONTENTS

LIST OF FIGURES

LIST OF TABLES

CHAPTER I: INTRODUCTION

1.1 Skin Cancer Background

1.1.1 Introduction

It is estimated that diagnosed skin cancer cases accounted for roughly 5% of new cancer cases (Siegel, 2014) in 2014, however, those numbers do not include basal cell or squamous cell skin cancers which are often not reported to cancer registries (Siegel, 2014). Skin cancer diagnoses are primarily dived into two categories, melanoma and nonmelanoma skin cancer (NMSC). NMSC include both basal cell carcinoma (BCC) and squamous cell carcinoma (SCC) and are generally regarded as being more benign than melanoma cases which are responsible for the majority of mortalities related to skin cancer (Gilchrest, 1999).

1.1.2 Melanoma

Melanoma represents about 3% of all skin cancers but it accounts for roughly 75% of all skin cancer deaths (Gilchrest, 1999). The American Cancer Society estimated that in 2014 there were 76,100 new cases of melanoma skin cancer with 9,710 new deaths. The rate of mortality is high considering the fact that melanoma is nearly always curable in its early stages, however, late diagnosis often coincides with cancer metastasis

to other parts of the body increasing the risk of mortality. Moreover, even though skin cancers are not as prevalent in individuals with darker skin, the possibility of fatalities may be even greater, as they may go undiagnosed for some time (Siegel, 2014).

Over the last thirty years, the incidence and mortality rates of melanoma have increased in the U.S (Petermann, 2007). Melanoma most often appears on the torso of men and the lower legs of women (Petermann, 2007). While the development of the disease stems from several factors, the exposure to ultraviolet radiation (UVR) is a major contributor, with one study indicating that up to 90% of all melanoma cases are attributed to UVR exposure (Glanz, 2007).

1.1.3 Nonmelanoma

It is estimated that between 2 and 3 million cases of NMCs occur worldwide each year and over 1 million cases happen in the U.S each year (Narayanan, 2010). Approximately 30% of newly diagnosed cancers in the U.S are BCC, making it one of the most commonly diagnosed cancers in this country (Rittié, 2007). Due to the benign nature of NMSC, some patients may remain undiagnosed and unregistered to cancer centers which has led to an under-representation of the number of cases reported (Suárez, 2007). Additionally, NMSC tends to have localized symptoms that primarily manifest in the elderly population, resulting in further undiagnosed cases (Narayanan, 2010).

Both BCC and SCC are typically found in sun-exposed areas, primarily on the head and neck areas, although, rate of incidence is higher for women in both types of cancer on the legs (Diepgen, 2002). Additionally, some literature describes the effect of skin pigmentation in different populations, and its impact on skin cancer, with fair skinned populations seeing a higher rate of incidence. Like melanoma, both BCC and SCC have been found to be related to the amount of UVR exposure (Preston, 1992). Studies have indicated that the probability of SCC diagnoses is less than BCC, however, there is a 10-fold increase in metastasis and mortality with SCC diagnoses.

1.1.4 Ultraviolet radiation

UVR is divided into UVA (315-400 nm), UVB (280-315 nm), and UVC (100-280 nm) (Narayanan, 2010). Roughly 90% of the solar UVR that reaches the earth's surface is UVA with the remaining percentage being UVB. Direct exposure of UVR to the skin is believed to cause DNA damage, gene mutations, immunesuppression, oxidative stress and inflammation, all of which have been shown to play a role in the aging of skin and the formation of skin cancer (Meeran, 2008).

Studies have suggested certain life-style changes that limit UVR exposure, including minimizing exposure to artificial UVR such as tanning beds and lamps, reduce the risk of NMSC. This study suggests that people who use artificial UV tanning have a 2-3 fold increased risk of NMSC (Karagas, 2002). Additionally, certain every day

strategies have been shown to reduce sun damage and increase the prevention of skin cancers. This includes, but is not limited to, minimizing sun exposure during peak hours, the use of sun-protective clothing, and applying a sun screen that blocks both UVA and UVB (Narayanan, 2010).

1.2 Topical Drug Delivery

1.2.1 Skin Anatomy

The skin is a multilayered organ with a total thickness of 2-3 mm. A cross section of the skin along with typical UVA/B penetration sites can be seen in Figure 1.1. The epidermis is the most proximal layer and is approximately 100 μm thick. The epidermis can be further subdivided into several layers, such as the stratum germinativum, which is the basal layer of the epidermis, and the stratum corneum (SC), the most proximal layer (Holbrook, 1993).

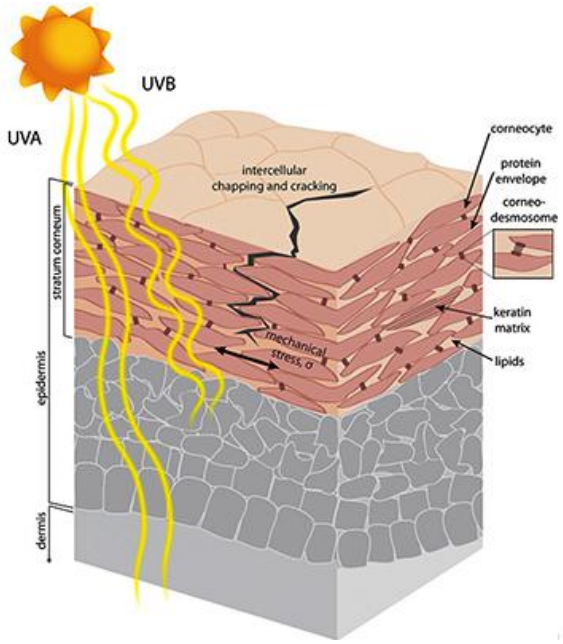

Figure 1.1 Cross section of the human skin and penetration sites of different UV wavelengths (Biniek, 2012).

New skin cells are formed at the basal layer and slowly move toward the surface. Upon arrival, epidermal cells are cornified and flattened where they are shed from the skin at a rate of about one cell layer per day (Ghosh, 1997). The SC is roughly 12-20 μm thick and covers most of the human body and represents the main resistance to penetration and permeation through the skin (Ghosh, 1997). One reason for this is that the skin cells at the surface are flat, creating a brick like barrier to the membrane. These cells contain fewer lipids than lower levels and those lipids are primarily free sterols, free fatty acids, and triglycerides (Lampe, 1983).

1.2.2 Topical Delivery

Topical formulations are intended to treat cutaneous conditions. Formulations are designed to deliver drugs locally, focusing on the tissue directly under the application or in deeper regions a bit further from the application site. As little as 1% and as much as 15% of the drug becomes bioavailable from topical formulations (Ademola, 1997). However, topical formulations allow for high local drug levels while maintaining lower drug levels in the surrounding region. In most instances, systemic uptake is unavoidable but tends to have minimal impact. Likewise, local administration of a topical formulation allows for greater drug concentrations to reach the afflicted area compared to a systemic delivery route (Ademola, 1997). The most common forms of topical formulations are ointments and creams, however, other delivery systems exist, such as gels, solutions and lotions.

Drug release from topical formulations involves partitioning of the drug from the vehicle into the SC, followed by passive diffusion through the skin. Physiochemical properties of the drug, vehicle, skin and the interactions between them affect the release of drugs from topical formulations (Barry, 1993). These interactions can be complex but in general, the driving force of drug release is dependent on permeability and solubility.

CHAPTER II: PREFORMULATION OF SULFORAPHANE

2.1 Background

2.1.1 Drug properties

Chemical Name: 1-Isothiocyanato-4(methlysulfinyl)-butane

Chemical Formula: $C_6H_{11}NOS_2$

Molecular Weight: 177.29 g/Mol

Boiling Point: 125°C

Calculated Log P: 0.23

Appearance: Viscous yellow liquid at room temperature

Chemical Structure:

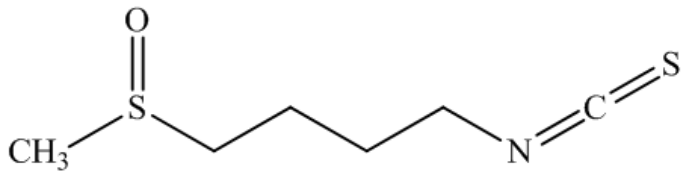

2.1.2 Role in skin cancer

Sulforaphane (SFN), a naturally occurring isothiocyanate (1-Isothiocyanato-4(methlysulfinyl)-butane) found in cruciferous vegetables such as broccoli, has been investigated in preclinical and clinical studies as a chemopreventive agent that may show effectiveness against ultraviolet (UV)-induced skin carcinogenesis (Dickinson, 2009). SFN is commonly known as a strong inducer of cytoprotective enzymes through induction of the phase II detoxification response and antioxidants; SFN activates the Nf-E2-related factor 2 (Nrf2) transcription factor, which binds to the Antioxidant Response Element (ARE) site in the promoter of many genes involved in cellular protection. Through the regulation of transcription linked to the ARE, Nrf2 can also regulate inflammation, phase I metabolism enzymes, the cell cycle, and apoptosis (Juge, 2007). Another mechanism of action of SFN is its ability to inhibit the activity of the activator-protein-1 (AP-1) transcription factor. AP-1 is strongly activated by treatment of keratinocytes with ultraviolet irradiation, particularly UVB (Chen, 1998). Dysregulation of AP-1 signaling during cancer progression can lead to alterations in cellular proliferation, apoptotic responses and differentiation. Inhibition of AP-1 greatly reduces UVB-induced skin carcinogenesis in mice (Cooper, 2003; Barthelman, 1998; Li, 1996). Recently it has been shown that SFN inhibits AP-1 activity by directly binding to its DNA binding domain, therefore preventing the protein from interacting with its response element, the TRE, in the promoters of AP-1 regulated genes (Dickinson, 2009). It has

also been shown that SFN effectively inhibits UVB-induced skin carcinogenesis in mice (Dickinson, 2009; Dinkova-Kostova, 2006).

2.1.3 Specific Aims

Despite evidence provided in the literature demonstrating SFN's promise as a chemopreventive agent for skin cancer, few studies have been conducted investigating potential topical formulations. So far, all topical interventions using SFN on mice and human subjects have involved dissolving SFN in acetone or an acetone/water mixture (Dinkova-Kostova, 2007; Talalay, 2007). In order to translate these findings into longer-term clinical trials, a topical formulation that is easily applied to the skin and does not cause irritation is required. The formulation needs to efficiently deliver SFN to the epidermis. It must also afford stability over the long term.

There is little data available concerning the stability of SFN as a function of pH, temperature, and in various solvents that would prove beneficial in developing a suitable formulation for preclinical and clinical trials. Because SFN has been observed to be highly unstable in water at elevated temperatures (Jin, 1999), traditional topical vehicles which usually contain high water content are likely not feasible vehicles for SFN. Thus, non-aqueous conditions needed to be explored.

The purpose of this study is to:

- Investigate the stability of SFN under various pH conditions
- Investigate the stability of SFN under various temperature conditions
- Investigate the stability of SFN in various solvent vehicles
- Investigate the stability of SFN in two non-aqueous formulations
- Evaluate the non-aqueous formulations to determine a potential lead formulation
- Determine the efficacy of the lead formulation *in vivo* in an AP-1 luciferase mouse model

2.2 Materials

Sulforaphane was procured from LKT Laboratories (St. Paul, MN, USA). Monobasic potassium phosphate, dibasic sodium phosphate, sodium citrate, boric acid, hydrochloric acid, ascorbic acid, polyethylene glycol (PEG) (200, 300, 400, 600), mineral oil, butylated hydroxytoluene, HPLC grade isopropyl alcohol, ethylenediaminetetraacetic acid disodium salt: dihydrate (EDTA), methanol and triethylene glycol dimethyl ether (Triglyme), were purchased from Sigma-Aldrich (St. Louis, MO, USA). Citric acid, stearic acid, and isopropyl palmitate were acquired from Spectrum Chemical Company (New Brunswick, NJ, USA). Sodium hydroxide was obtained from EM Science (Darmstadt, Germany). Ethyl alcohol (200 proof) was bought from Aaper Alcohol and Chemical Co. (Shelbyville, KY, USA). Bath oil was purchased from Pharmaceutical

Specialties (Rochester, MN, USA). HPLC grade acetonitrile was acquired from EMD (Gibbstown, NJ, USA). PPG-2 myristyl ether propionate was obtained from Croda (Edison, NJ, USA). PEG ointment base was bought from Lab Express International (Fairfield, NJ, USA). A Millipore water purification system with a 0.22µm filter was used for water.

2.3 Experimental

2.3.1 High performance liquid chromatography (HPLC)

Samples were analyzed with a Waters System consisting of a 2690 Alliance separation module, coupled with a 996 Photodiode Array Detector (Waters Corporation, Milford, MA). Separation was achieved using a 150mm × 3.9mm Altima C18 5µm column maintained at 30ºC. Ultraviolet detection was done at 241nm. A reverse phase HPLC method was developed to analyze drug concentrations from a variety of experimental conditions. Aqueous samples and solvent stability utilized an isocratic acetonitrile:water (76:24) run for 14 minutes. Topical formulations used one of two gradient methods to ensure that residual formulation components were removed from the column. Polyethylene glycol (PEG) formulations followed the initial isocratic conditions described above followed by a linear ramp to acetonitrile:water (10:90) over 10 minutes proceeded by a 2 minute linear ramp returning to the original isocratic conditions. Organic oleaginous formulations also utilized the isocratic conditions followed with a

linear ramp to 100% isopropyl alcohol for 10 minutes and then a linear ramp of 2 minutes resuming to the initial mobile phase conditions. Total run time was 35 minutes for analysis of both topical formulations. Standards were prepared from a roughly 500 µg/ml stock solution of SFN in 100% acetonitrile (ACN) and ranged from 2.5-200 µg/ml. The retention time for SFN was approximately 8 minutes for all formulations. Samples were run with a constant flow rate of 0.45mL/min and an injection volume of 10µL. All quantifications were based on peak area.

2.3.2 Mass Spectrometry (MS)

Analysis of SFN was carried out on a TSQ Quantum triple quadrupole LC-MS with a Surveyor MS pump and Surveyor autosampler (Thermo Finnigan, San Jose, CA). Chromatographic separation was achieved using the isocratic method described above with the exception of a Waters Symmetry column (150mm × 3.9mm C18 5µm) used in place of an Altima. The mass spectrometer was operated in electrospray positive ionization mode with a spray voltage of 4500V, sheath gas flow of 20 arbitrary units (au), auxiliary gas flow of 3au and ion transfer capillary temperature of 350°C. Detection was by full scan MS mode, scanning from 150 to 1000 m/z.

2.3.3 Stability Studies

2.3.3.1 Effect of pH

The effect of pH on the stability of SFN was determined using a citrate buffer in the pH range of 4-5, a phosphate buffer in the pH range 5-8, and a borate buffer at pH 9. Buffers were prepared at a 0.1M concentration and with a constant ionic strength of 0.1M. Buffers were pH adjusted with NaOH and HCl as needed and samples (n=2) were prepared with ACN as a cosolvent at 20% (V/V). The target concentration of SFN was 200 µg/ml and degradation was observed over four weeks at 4, 26, 56 and 65°C. Stability was determined using HPLC isocratic conditions mentioned above.

2.3.3.2 Effect of solvents

The impact of different organic solvents on the stability of SFN was investigated at an elevated temperature (37°C) in order to observe drug degradation in an accelerated manner. A target concentration (200 µg/ml) of SFN was introduced to several organic solvent environments, including acetonitrile (ACN), ethanol (EtOH), isopropanol (IPA), methanol (MeOH), and triglyme.

Additionally, the degradation rate of SFN was observed in water (H_2O, pH=8) as well as in a neat solution of pure SFN. In an attempt to stabilize degradation the effect of

a chelating agent, EDTA (0.05M, pH=8), was also studied. Degradation was analyzed over a week long period and samples (n=2) were assayed using HPLC isocratic conditions stated above.

2.3.3.3 Stability in topical vehicles

Initial formulation stability was conducted with a variety of topical vehicles at room temperature. Initially, SFN stability was observed in isopropyl palmitate, PEG 400, bath oil composed of cotton seed oil and alkyl aryl polyether alcohol, as well as in a more conventional oil-in-water cream (Gupta, 2004). Samples (n=2) were prepared at a target concentration of 1% wt/wt and observed over the course of five months.

2.3.3.4 Effect of PEG Chain length

The relationship between stability and PEG chain length was investigated. A target concentration (200 µg/ml) of SFN was introduced into pure PEG formulations that included PEG 200, 300, 400, and 600. To understand the potential effect of the polymer chain length, the stability of SFN in the structural subunit ethylene glycol was also investigated in a similar manner. Furthermore, to understand the potential impact of water in the formulation, a series of PEG 400 that contained additional water (0.1% and 1.0% wt/wt) was investigated. Stability was conducted at an elevated temperature of 37°C for one week (n=2).

2.3.4 Topical formulations: preparation

Based on resultant data from the initial formulation screening, two non-aqueous topical formulations were considered for further evaluation. A PEG ointment base (60% PEG 400 and 40% PEG 3350) and an organic oleaginous base composed of the organic components from the previously mentioned oil-in-water cream (39% stearic acid, 35% isopropyl palmitate, 17% mineral oil, 9% PPG-2 myristyl ether propionate) were utilized. These formulations were prepared by manually compounding roughly 4.4 mg of SFN per gram of base formulation. Once mixing was achieved stock material was aliquoted into three equal portions. Additionally, the effects of antioxidants on stability were studied by adding 0.1% of either ascorbic acid or butylated hydroxytoluene (BHT) to the separate aliquots of formulation. Stability was conducted at 4, 26, 56 and 65°C.

2.3.5 Effect of temperature

The impact of temperature on the degradation rates of SFN were observed at four different temperatures (4, 26, 56, and 65°C) in two non-aqueous topical formulations. Analysis of the degradation rates of SFN at different temperatures allows for the estimation of activation energy.

Sampling frequency was dependent upon temperature exposure. Formulations at higher temperatures (56°C and 65°C) were sampled every few days for up to six weeks or

until drug was depleted. At lower temperatures (4°C and 26°C) formulations were sampled every few weeks, often only once a month. Due to the higher drug concentration that remained under these conditions, stability was observed over a six month period.

Drug content was analyzed by sampling 7-10 mg of formulation and placing it directly into an HPLC vial (n=2). One milliliter of solvent, isopropyl alcohol for the organic oleaginous formulation and oil-in-water cream, and acetonitrile for the PEG formulation and remaining pre-formulation samples, was added to the HPLC vials. Vials where shaken to ensure complete dissolution then analyzed by the HPLC conditions mentioned above.

2.3.6 In Vivo Studies

Mice were housed in accordance with The University of Arizona Animal Care and Use Committee standards. Female SKH-1 mice expressing TRE-driven luciferase (AP-1 luciferase mice) (Cooper, 2003; Rincon, 1994) were separated into two groups of 10 animals each. The skin of both ears per mouse was treated with the PEG ointment base with or without the addition of SFN four times (day 1, 3, 5 and 8). Punches were taken from the right ear on day 9 (pre-UV samples). Mice were all treated with an acute dose of 2.75 kJ/m^2 UVB on day 10 and then treated with vehicle or drug again about 30min after UVB exposure. The source of UVB was a bank of six FS40T12 UVB lamps (National Biological Corporation, Beachwood, OH). Forty-eight hours after UVB

treatment (day 12), all mice were sacrificed and punches were taken from the left ear of each mouse (post-UV samples). Ear punches were flash frozen in liquid nitrogen and stored at -80˚C until processing for the luciferase assay as described previously (Bachelor, 2005). Ten micrograms of protein per sample was used to perform the luciferase assay. Post-UV luciferase activity was divided by Pre-UV luciferase activity for each individual to calculate fold-activation. Outliers were dropped if their post/pre luciferase ratio was more than two standard deviations away from the mean (final n = 8 for both groups). *In vivo* studies were conducted by Dr. Sally Dickinson from the University of Arizona Cancer Center.

2.4 Results and discussion

2.4.1 Mass spectrometry (MS) analysis

Initial analytical standard solutions were prepared in methanol. However, an additional peak, at 5.5 minutes, was observed in the HPLC chromatograms of samples in methanol, thereby prompting further analysis. Mass spectrometry analysis of these samples identified that SFN eluted at 10.3 minutes with an m/z of 177.91 (Figure 2.1). Analysis also showed a methanol solvolysis product with an m/z of 209.93 from the degradation peak seen at 5.5 minutes (Figure 2.2).

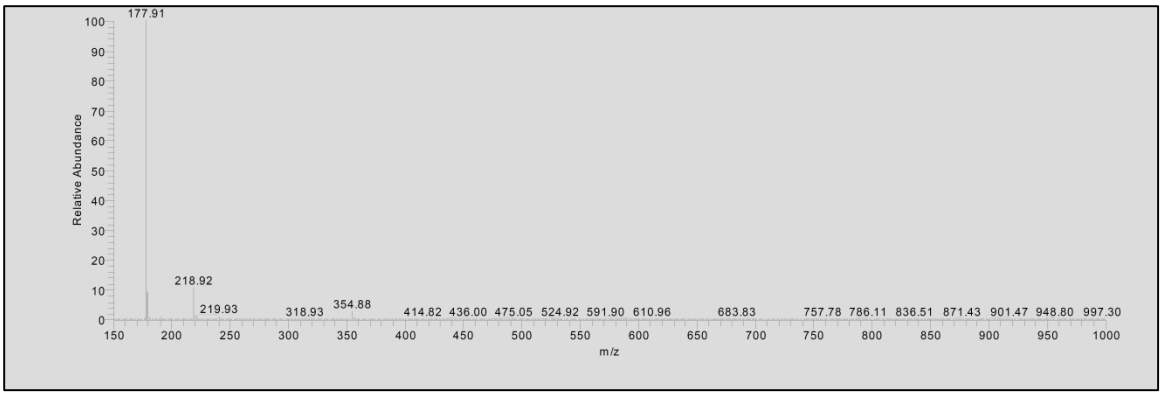

Figure 2.1 Mass spectrometry of SFN, elution at 10.3 min.

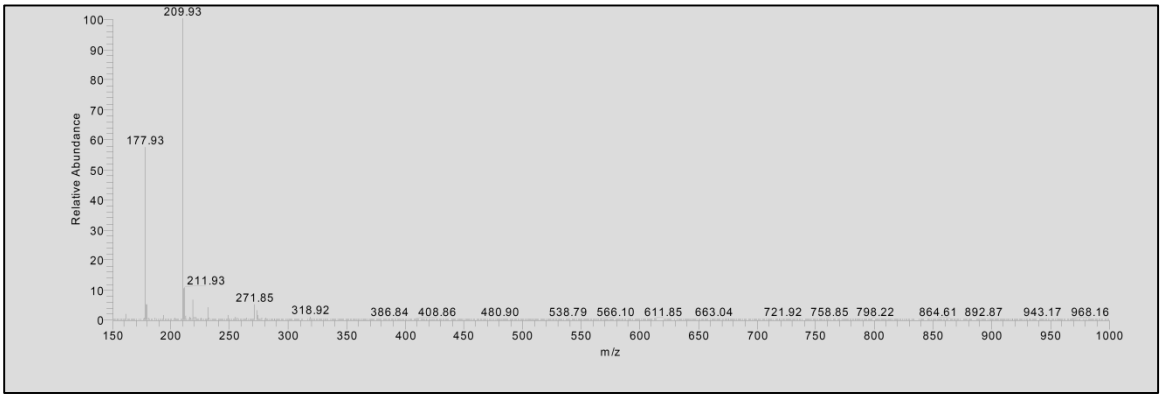

Figure 2.2 Mass spectrometry of methanol solvolysis product, elution at 5.5 min.

In addition, the presence of the thiourea, N,N'-di-(methylsulfinyl) butyl thiourea (SFN dimer), previously discussed (Jin, 1999) was also confirmed in these samples (m/z= 312.94) at 2.9 minutes (Figure 2.3). Following MS analysis, future analytical standards were prepared in ACN.

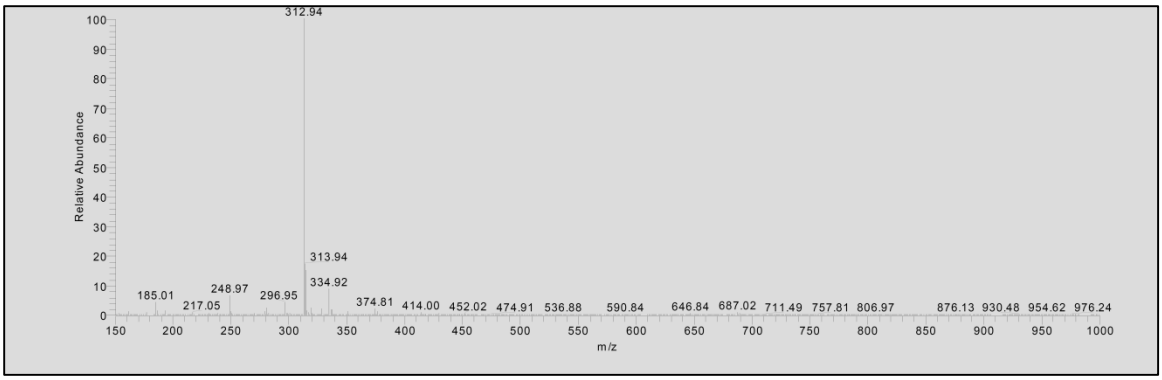

Figure 2.3 Mass spectrometry of thiourea, N, N'-di-(methylsulfinyl) butyl thiourea, elution at 2.9 min.

2.4.2 Stability Studies

2.4.2.1 Effect of pH

Drug stability can be altered by different pHs, catalyzed by either hydrogen ions or hydroxide ions and in some cases both. Stability of SFN was tested under seven different pH conditions ranging from 4-9 and utilizing a variety of buffer species (citrate, phosphate, borate), at 26°C and a constant ionic strength of 0.1M. The kinetic rate profile can be seen in Figure 2.4 (citrate data not shown).

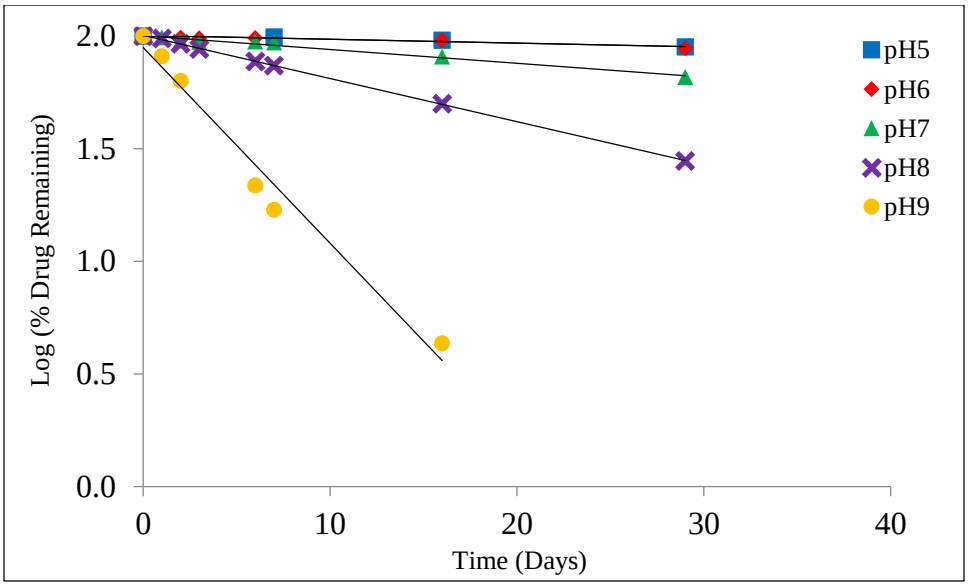

Figure 2.4 Log percent (%) drug remaining versus time at various pHs (26°C) (citrate data not shown).

From the kinetic rate profiles it is evident that the degradation of SFN undergoes apparent first-order kinetics in the pH conditions presented. The degradation rate constants (κ) were calculated from the slope of the log-linear best fit (regression) line by the following equation.

$$\kappa = -Slope \times 2.303 \qquad \text{Eqn. 2.1}$$

Rate constants were used to plot a pH-rate profile (Figure 2.5) for SFN at 26°C that indicates that SFN undergoes base-catalyzed degradation.

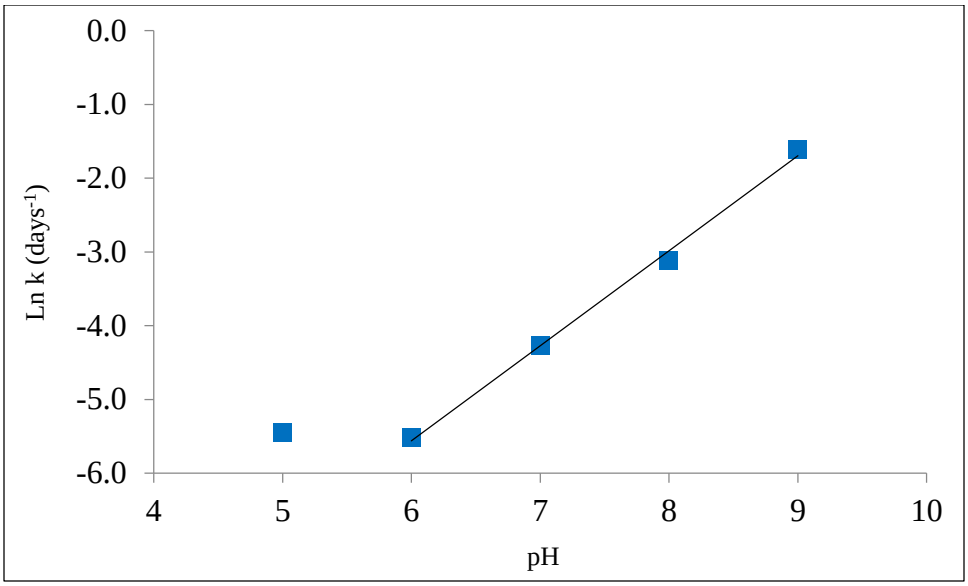

Figure 2.5 SFN pH-rate profile, natural logarithm of the degradation rate constant (κ) versus pH (26°C) (citrate data not shown).

These results are consistent with other reports, which monitored stability as a function of pH for 2 hours at elevated temperatures (Xiao, 2009). Interestingly, the slope from pH 6 to pH 9 is 1.29; potentially indicating that in addition to base-catalysis there may be other mechanisms occurring.

From the degradation rate constant, half-life (T_{50}) and shelf life (T_{90}), defined as the time at which 10% of the drug has degraded, can be calculated. These values can be obtained by Equation 2.2 and 2.3, respectively. A summary of the data can be seen in Table 2.1.

$$\frac{0.693}{\kappa} = T_{50} \qquad \text{Eqn. 2.2}$$

$$\frac{0.105}{\kappa} = T_{90} \qquad \text{Eqn. 2.3}$$

pH	κ (per day)	$\mathbf{T_{50}}$(days)	$\mathbf{T_{90}}$(days)
4 (Citrate)	0.044	15.8	2.4
5 (Citrate)	0.071	9.8	1.5
5 (Phosphate)	0.004	161.2	24.4
6 (Phosphate)	0.004	173.3	26.3
7 (Phosphate)	0.014	49.2	7.5
8 (Phosphate)	0.044	15.7	2.4
9 (Borate)	0.200	3.5	0.5

Table 2.1 Degradation rate constant, half-life, and shelf life for SFN at various pHs.

It is clear, based on the pH 4 and pH 5 data, that buffer species can have an impact on SFN degradation. The data for pH 4 and 5 in citrate buffer are not included in Figures 2.4 and 2.5. Those results are discussed below in *Effect of buffer species*. No pH change was noted in any of the samples over the course of the study.

2.4.2.2 Effect of buffer species

The effect of buffer species was determined at pH 5 in 0.1M citrate and 0.1M phosphate buffers at 26°C (ionic strength of 0.1M). SFN was observed to undergo apparent first-order degradation regardless of buffer species (Figure 2.6).

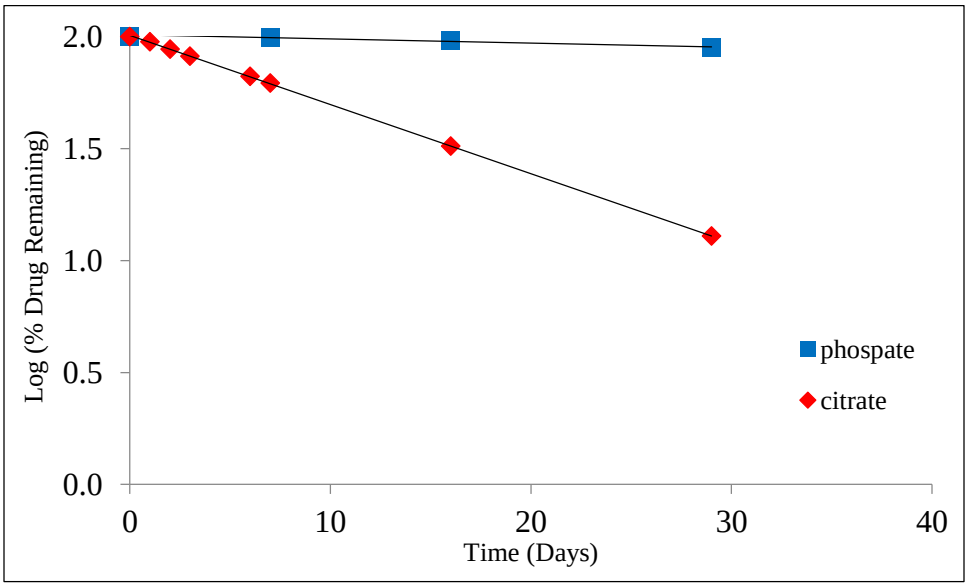

Figure 2.6 Effect of buffer species (pH=5) on SFN stability (26°C).

After 30 days of buffer exposure approximately 89.6% of SFN remained in the phosphate buffer with a κ value of 0.004 (per day) and a T_{90} of 24.4 days. In comparison, roughly 12.9% of SFN remained in the citrate buffer after 30 days with a κ value of 0.071 (per day) and a T_{90} of 1.5 days. Additionally, when SFN was exposed to a citrate buffer of pH 4 (ionic strength of 0.1M), similar trends were seen as compared to the pH 5 citrate buffer. At pH 4, 28.7% of SFN remained after 30 days with a κ value of 0.044 (per day)

and a T_{90} of 2.4 days. Thus, it appears that the SFN degradation rate constant remains relatively constant between pH 4 and 5, however it was clear from this observation that SFN is more stable in phosphate buffer compared to citrate buffer. The drastic difference in stability as a function of buffer species should be taken into consideration as formulations are developed.

2.4.2.3 Effect of solvents

The stability of SFN was investigated in five different organic solvents; ACN, EtOH, IPA, MeOH, and Triglyme. In addition, stability was conducted in H_2O, H_2O with EDTA, and a neat solution of pure SFN. These samples were evaluated at 37°C over the course of one week and the results are given in Figure 2.7.

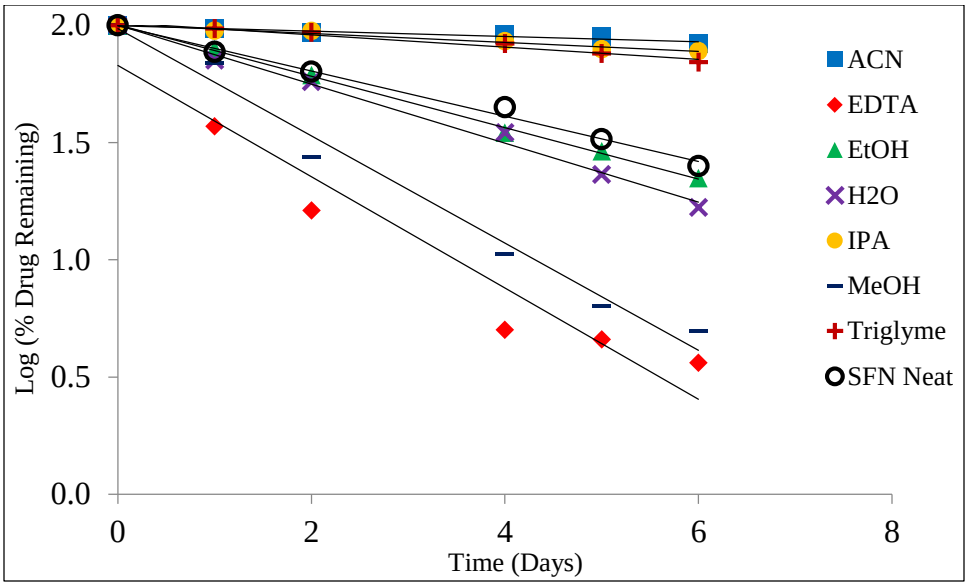

Figure 2.7 Log percent (%) of drug remaining in a variety of solvents, and in a neat solution (37°C).

From the data it can be observed that SFN is relatively stable in ACN, IPA and Triglyme, less stable in EtOH, H_2O and the neat solution, and SFN degraded the fastest in the EDTA solution and MeOH. This indicates that SFN degradation is influenced by the type of polar protic solvent. The two polar aprotic solvents, ACN and Triglyme, were two of the three solvents in which SFN had the greatest stability. Indeed, this is relative as the ACN sample still had 83.5% remaining and triglyme had 70.0% remaining after 6 days. The third solvent in which stability was relatively higher was the tertiary alcohol IPA. However, as the polarity of the alcohol series increased, from IPA to EtOH to MeOH, the stability of SFN dramatically decreased. Samples in IPA had 77.7 % remaining after six days and EtOH had 22.3% drug remaining after six days while samples in MeOH only had 2.5% remaining. Since SFN significantly degrades in pure organic environments, it is

clear that mechanisms other than simple hydrolysis are important to consider. Attempts to identify some of the degradation products from the organic stability samples were not successful at this time; however some possible mechanistic pathways have been previously reported, proposing that SFN degrades to a thiourea compound via hydyolsis (Jin, 1999).

In Millipore H_2O (pH=8, no buffer), approximately 57.5% of SFN remained after two days and had a calculated T_{90} of 0.8 (days) whereas, H_2O with EDTA (0.05M, pH=8) yielded 16.3% SFN remaining after two days and a T_{90} of 0.4 (days). Interestingly, while those H_2O samples displayed high levels of degradation, SFN stability conducted in phosphate buffer (pH=8) demonstrated even greater instability with 6.4% drug remaining after two days and a T_{90} of 0.19 (days). Furthermore, the inherent instability of SFN is evident by the degradation observed by the neat SFN sample. Pure SFN alone degraded 74.9% after 6 days at 37°C.

2.4.2.4 Stability in topical vehicles

The preformulation studies indicate that SFN is very unstable not only in aqueous and protic solvents, but also in polar aprotic environments. As such, attempts to formulate SFN in an oil–in-water cream formulation were unsuccessful. In fact, as illustrated in Figure 2.8, SFN completely degraded after 30 days in a conventional pharmaceutical

cream formulation. However, improved stability was observed in organic formulation components.

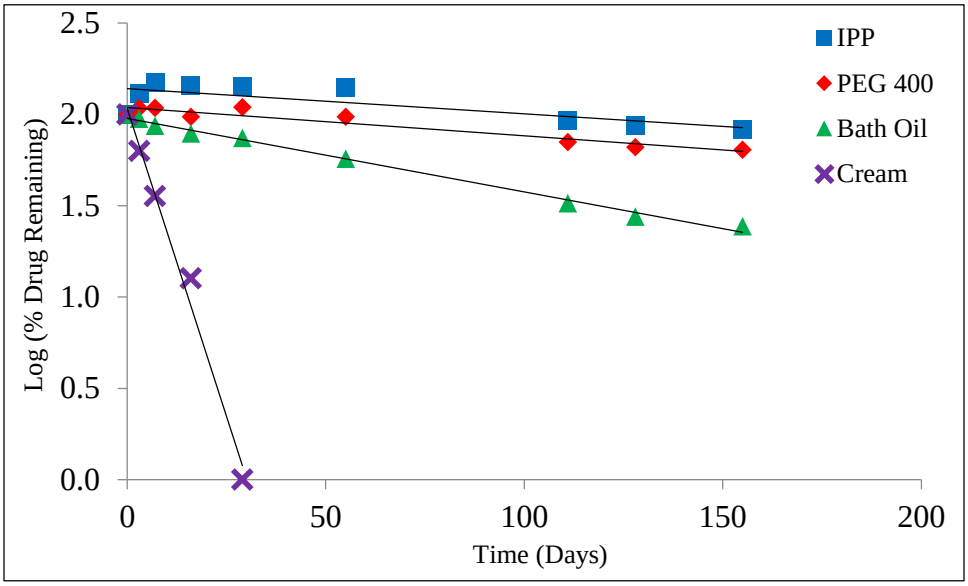

Figure 2.8 SFN preformulation stability studies (26°C).

Following the initial observations of stability in PEG 400, SFN stability was further investigated using a variety of PEG chain lengths (Figure 2.9). It was observed that SFN has greater stability in longer polyethylene glycol chain lengths such as PEG 600 and PEG 400 as compared to the shorter chain lengths of PEG 200 and PEG 300. Approximately 83.1% of drug remained in PEG 400 samples after 6 days at 37°C. In comparison, 50.5% drug was remaining in PEG 300 samples under similar conditions. Consistent with the above, SFN degraded rapidly (8.7% remaining after 6 days at 37°C) in the polar protic solvent ethylene glycol, which is the structural repeating unit of the PEG series.

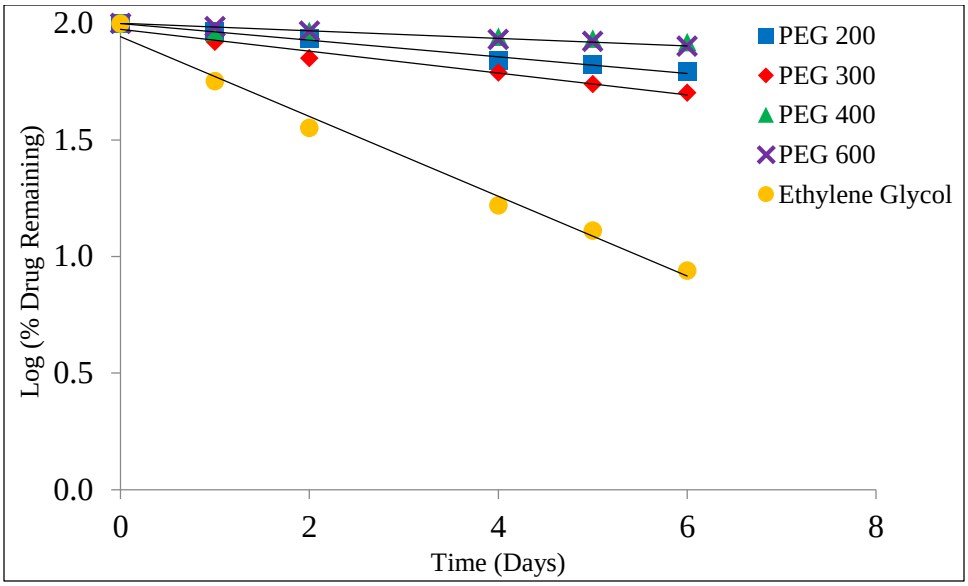

Figure 2.9 SFN stability in PEG with increasing chain length (37°C).

To understand the influence that H_20 may have on degradation of SFN when it is present in an organic solvent as an impurity, a water spiking study was conducted. PEG 400 samples were spiked with 0.1% and 1.0% water. Figure 2.10 shows that as water content increased, degradation rate also increased, albeit with minimal impact over the course of this particular study. After 6 days, the increase of water content from 0% to 1% increased the degradation from 14.9% to 19.3% at 37°C.

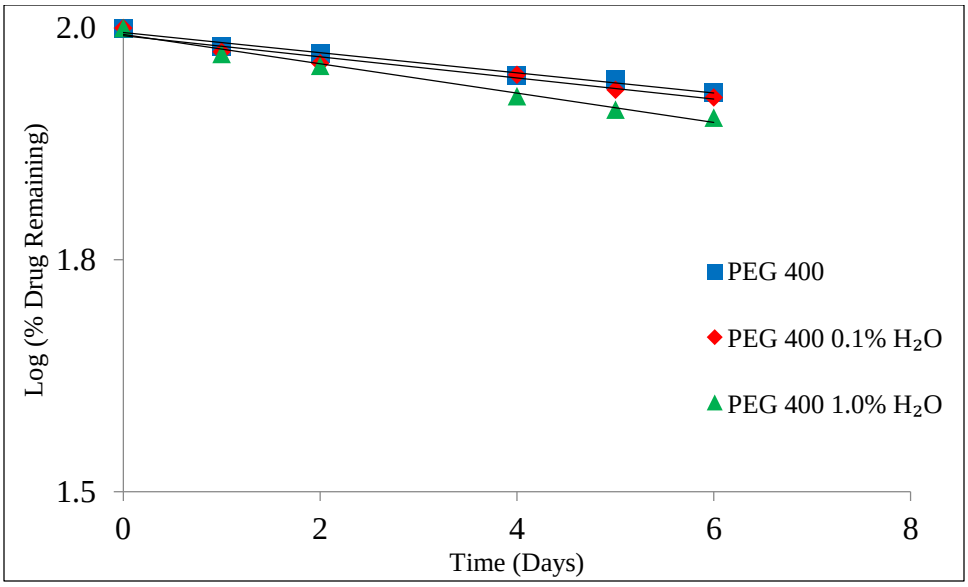

Figure 2.10 SFN stability in PEG 400 with increasing water content (37°C).

2.4.2.5 Stability in topical formulations

As a result of the preliminary stability studies, a PEG ointment base and an organic oleaginous base were selected for further stability investigations. Once again the stability of SFN is highly temperature-dependent with rapid degradation observed at higher temperatures in both formulations. However, an increase in stability was observed at lower temperatures (26°C and 4°C) (Figure 2.11 & 2.12).

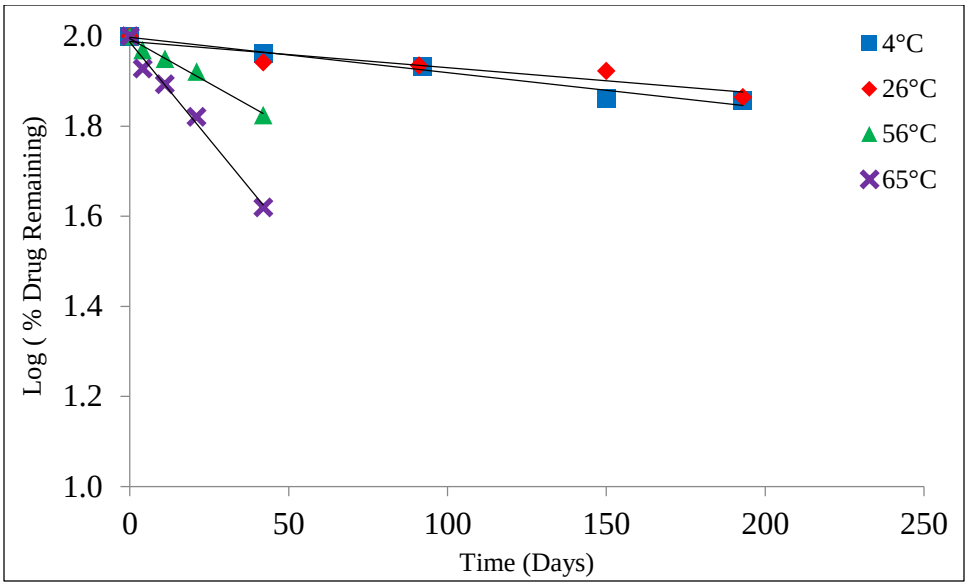

Figure 2.11 SFN stability in organic formulation at various temperatures.

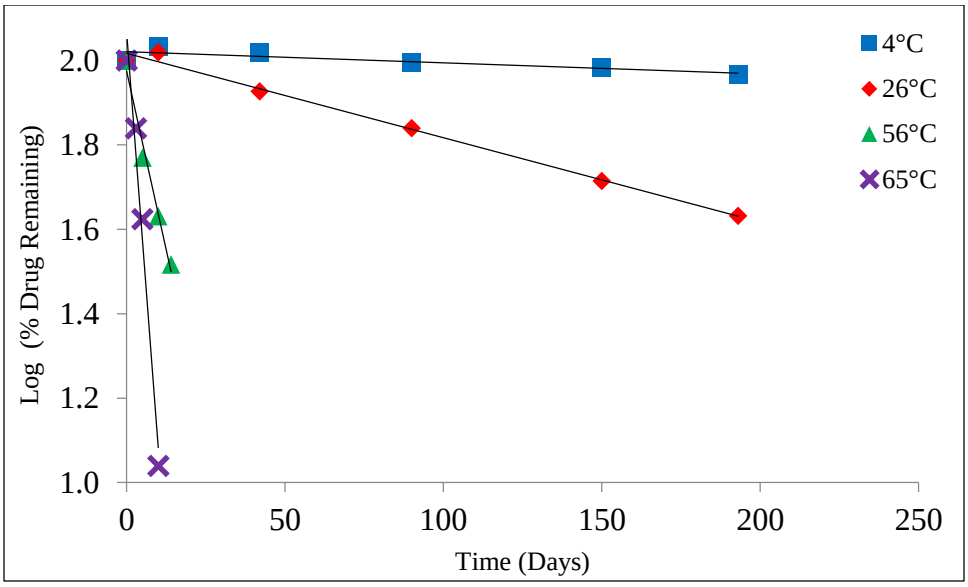

Figure 2.12 SFN stability in PEG formulation at various temperatures.

At 26°C, approximately 73.1% SFN remained in the organic oleaginous base after 193 days compared to 42.8% remaining in the PEG base. At 4°C, roughly 71.9% SFN remained in the organic oleaginous base after 193 days compared to 92.6% remaining in the PEG base. The addition of the anti-oxidant ascorbic acid (AA) improved the stability of the PEG formulation (Figure 2.13) particularly at lower temperatures, 95.3% remaining after 193 days at 4°C, but had no effect on the organic oleaginous base formulation. Conversely, the addition of the anti-oxidant BHT provided no improved stability in either formulation (data not shown). Although there is SFN degradation in these non-aqueous formulations, they are appreciably more stable than the solution studies previously described.

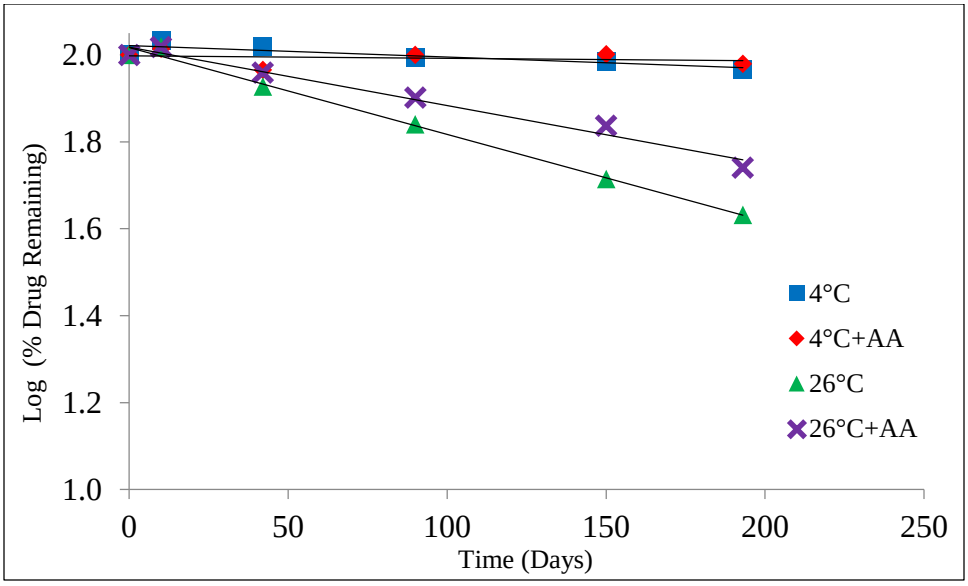

Figure 2.13 Effect of ascorbic acid (AA) on SFN stability in PEG formulation.

2.4.2.6 Effect of temperature

The degradation rate constants are related to temperature by the Arrhenius equation, seen below.

$$k = Ae^{-Ea/RT} \quad \text{Eqn. 2.4}$$

Where κ is the degradation rate constant, A is the collision factor, Ea is the energy of activation, R is the gas constant and T is the temperature in Kelvin. This equation can be expressed in either a logarithm (Eqn. 2.5) or natural logarithm (Eqn. 2.6) form.

$$Log\ k = \log A - \frac{Ea}{2.303}\frac{1}{RT} \quad \text{Eqn. 2.5}$$

$$Ln\ k = -\frac{Ea}{R}\frac{1}{T} + \ln A \quad \text{Eqn. 2.6}$$

Equation 2.6 is typically plotted as Ln κ as a function of 1/T. The linear regression of the best fit line can then allow for the calculation of the activation energy through Equation 2.7.

$$Ea = -Slope \times 0.008314 \quad \text{Eqn. 2.7}$$

The activation energy can then be substituted into Equation 2.6 and drug stability can then be estimated at any temperature, assuming the degradation mechanism remains constant over the given temperature range.

The Arrhenius relationship (Figure 2.14) demonstrates the difference in degradation rate of the two formulations as a function of temperature. At high temperatures (56°C and 65°C) a larger percent of drug remained within the organic oleaginous base formulation compared to the PEG base formulation. Interestingly, the results are reversed at lowest temperature (4°C) with a greater percent of drug remaining in the PEG formulation.

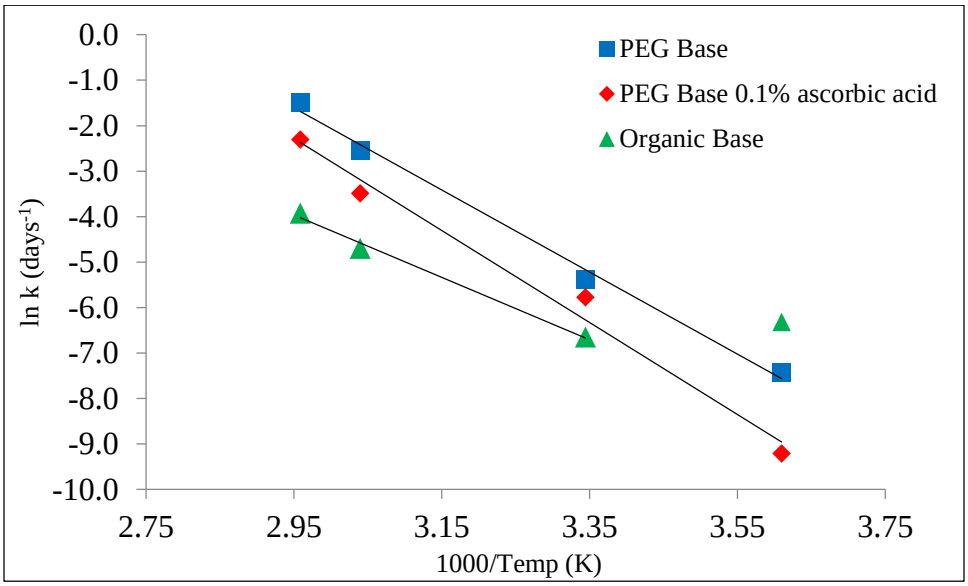

Figure 2.14 Arrhenius plot: temperature effect on SFN formulation stability.

While activation energy is a useful metric to interpret stability data, in this instance careful consideration should be made when drawing definitive conclusions. Throughout the course of the study it was observed that both the PEG ointment base and organic oleaginous base had changes to their physical nature depending on the storage temperature. The PEG formulations become significantly less viscous at higher temperatures, whereas the oleaginous base became semi-solid at 4°C. SFN in PEG base alone had a calculated *Ea* of 75 kJ/mol and a T_{90} of 175 days at 4°C. As a result of the changes seen to the organic oleaginous base at 4°C, the *Ea* for that formulation can be calculated with or without that data point. The inclusion of that data results in an *Ea* of 32 kJ/mol and T_{90} of 58 days at 4°C. The degradation rate, half-life, and shelf life for 4°C and 26°C, as well as the activation energy for each formulation can be seen in Table 2.2.

Formulation	κ (per day)	T_{50}(days)	T_{90}(days)	***Ea***(kJ/mol)
PEG Base	-	-	-	75
4°C	0.0006	1155	175	-
26°C	0.0046	150	22	-
PEG + AA	-	-	-	84
4°C	0.0001	6930	1050	-
26°C	0.0031	223	33	-
Organic Base	-	-	-	-
(4° data included)	-	-	-	32
(4° data **not** included)	-	-	-	57
4°C	0.0018	385	58	-
26°C	0.0013	533	80	-

Table 2.2 Degradation rate, half-life, and shelf life (4°C and 26°C), as well as the formulation activation energy.

2.4.3 In vivo experiments

To test the ability of the above formulations to affect targets *in vivo*, the PEG ointment base was tested on the skin of hairless AP-1 luciferase mice. The ears of hairless mice transgenic for an AP-1 driven luciferase gene were pretreated with either PEG ointment (vehicle) or the ointment containing SFN 4 times prior to and 1 time 30 minutes after an acute treatment with UVB. Ear punches were taken 24 hrs before and 48 hrs after UVB treatment. As has been previously reported, acute UVB treatment of AP-1

luciferase mice yielded strong activation of the luciferase transgene in the skin of placebo treated controls (Dickinson, 2009). This stimulation was diminished ~2.5 fold in mice pretreated with the ointment containing SFN, a significant reduction in signaling ($p = 0.02$) (Figure 2.15). No adverse reactions were noted with treatment of placebo or SFN-containing PEG ointment base. This suggests that SFN in this formulation is functional *in vivo*.

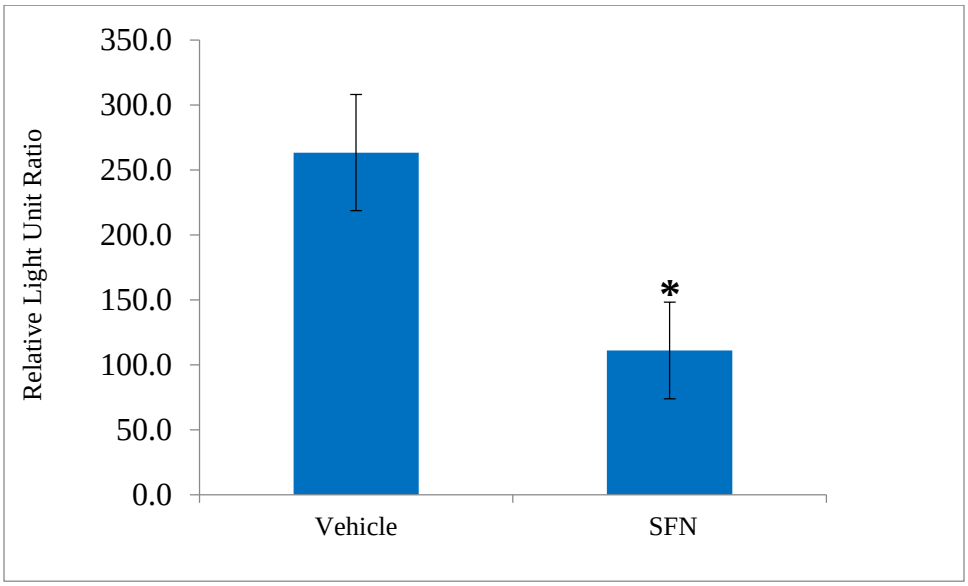

Figure 2.15 Fold-luciferase readings indicate that UVB significantly activated luciferase, and that this was significantly inhibited by treatment with SFN in the topical formulation ($p = 0.02$, $n=8$).

2.5 Conclusions

Preformulation studies have shown that SFN is chemically unstable not only in aqueous and protic solvents, but also in polar aprotic environments. It has been shown that SFN undergoes rapid apparent first order degradation under basic pH conditions as well as methanol solvolysis. At pH 5 and 26°C, SFN was found to be more stable in a phosphate buffer as compared to a citrate buffer system. SFN degradation is strongly dependent on temperature as evident by changes in the degradation rate constant as a function of temperature. For every 10°C change in temperature the degradation rate constant of SFN changed by a factor of 3.15 in a pH 4 solution and a factor of 4.0 for a pH 8 solution.

While SFN completely degraded after 30 days in a conventional pharmaceutical cream formulation, improved stability was seen in the organic formulation component PEG 400. It was observed that SFN stability in PEG is related to chain length with greater stability seen in longer PEG chain lengths. Long term stability studies were conducted on two non-aqueous topical formulations, a PEG ointment base and an organic oleaginous base. At 4°C, 92.6% of SFN remained in the PEG based formulation after 193 days. Topically applied SFN in the PEG formulation was then tested for efficacy and led to a significant decrease of luciferase transgene activation in an AP-1 luciferase mouse model compared to a vehicle control.

CHAPTER III: PREFORMULATION OF MYRICETIN

3.1 Background

3.1.1 Drug properties

Chemical Name: 3, 3', 4', 5, 5', 7-hexahydroxyflavone

Chemical Formula: $C_{15}H_{10}O_8$

Molecular Weight: 318.23 g/Mol

Melting Point: 357°C

Calculated Log P: -0.04

Experimental Log P: 2.94

Appearance: Yellow powder at room temperature

Chemical Structure:

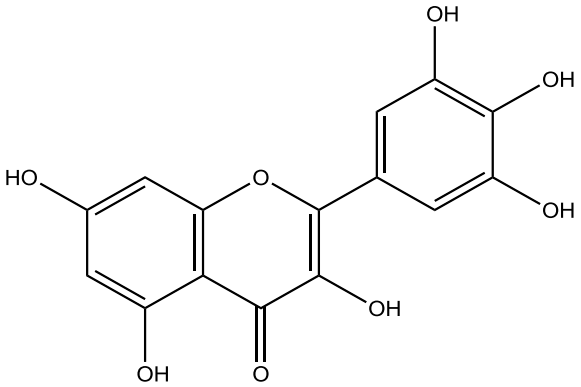

3.1.2 Role in skin cancer

Myricetin (MYR), is a naturally occurring flavonoid (3, 3', 4', 5, 5', 7-hexahydroxyflavone) found in a variety of fruits such as berries and grapes (Hakkinen, 1999; Hertog, 1993). Studies have identified flavonols, including MYR, to possess anti-oxidant, anti-tumor and anti-inflammatory activity (Surh, 2003; Ribeiro de Lima, 1999). The potential for dietary phytochemicals, such as MYR, as chemoprevention agents has been reported throughout the literature (Surh, 2003). With regard to MYR specifically, studies have demonstrated that MYR inhibits tumor cell transformation by direct inhibition of mitogen-activated protein kinase (MAPK)/ERK kinase (MEK) kinase activity in JB6 P+ mouse epidermal cells (Lee, 2007). This study also illustrated that the inhibitory effects of MYR were more potent than the well-characterized chemopreventive agent, resveratrol. Investigations into the role of MYR in skin cancer, including mechanism and target(s), indicate that MYR suppresses ultraviolet B (UVB) induced cyclooxygenase-2 (COX-2) protein expression in the same cell lines (Jung, 2008). Data suggests that this is achieved by MYR competitively binding to ATP to suppress Fyn kinase activity (Jung, 2008). Additionally, skin tumorigenesis data, via dorsal mouse skin, showed that pretreatment with a topical application of MYR in acetone reduced the incidence of UVB-induced skin tumors (Jung, 2008).

3.1.3 Specific Aims

Despite evidence in the literature demonstrating MYR's promise as a chemopreventative for skin cancer, as well as other indications (Li, 2012), minimal information is available to guide the progression of formulations designed for future drug development. One of the main issues facing potential formulations is the poor aqueous solubility often found amongst flavonoids. Quercetin (QT), a flavonoid similar in structure to MYR, has been reported to be fairly insoluble at room temperature (5.5 µg/ml) (Lauro, 2002). Likewise, MYR has also been shown to have low aqueous solubility at room temperature (< 1.5 µg/ml) (Hong, 2014) while *in vivo* experimentation indicated a low bioavailability of 9.6% in rats (Dang, 2013).

The high melting point of the crystal appears to be influential with respect to MYR's low solubility, while the non-polar log P suggests adequate permeability, thus MYR can be characterized as a class II compound by the Biopharmaceutics Classification System. As potential therapeutic benefits of MYR continues to be explored, so too does the approaches to enhance the solubility and absorption. Such delivery systems include complexation with β-cyclodextrins (Yao, 2014; Lucas-Abellan, 2008), a microemulsion (Wang, 2013), and the development of a 1:1 cocrystal with piracetam (Sowa, 2014).

In this study, data is presented that supports the existence of two hydrated forms of MYR which have not previously been reported. It has been estimated that one-third of

active pharmaceutical substances are capable of forming a hydrate (Qu, 2014). In most cases, hydrates contain water molecules within the crystal lattice that are bound at either isolated or channel sites (Brittain, 2009). The addition of the water molecule(s) in the crystal can alter the physical structure including changes to the shape, symmetry and capacity of the unit cell (Grant, 1995). These changes can lead to differences in pharmaceutical properties such as solubility and chemical stability (Grant, 1995). From a development perspective, an unexpected phase transition from anhydrous to the hydrate could lead to differences in product performance and alter the way a drug candidate is processed and formulated (Brittain, 2009).

The purpose of this study is to:

- Investigate the solid-state properties of MYR acquired from two vendors
- Investigate the solubility of the different crystal forms
- Investigate the dissolution profiles of the different crystal forms
- Investigate the stability of MYR under various pH conditions
- Investigate the stability of MYR under oxidation stress
- Investigate the stability of MYR under UV irradiation

3.2 Materials

Myricetin was purchased from both Research Products International (Mount Prospect, IL) and Sigma-Aldrich (St. Louis, MO). Monobasic potassium phosphate, dibasic sodium phosphate, sodium citrate, boric acid, hydrochloric acid, sodium chloride, ascorbic acid, sodium metabisulfite, polyethylene glycol (PEG) (200, 300, and 400), acetone, and 1-octanol were also purchased from Sigma-Aldrich. Citric acid, methanol, and propylene glycol were acquired from Spectrum Chemical Company (New Brunswick, NJ,). Sodium hydroxide was obtained from EM Science (Darmstadt, Germany). Ethyl alcohol (200 proof) was bought from Decon Labs (King of Prussia, PA). Acetic acid was bought from Fisher Scientific (Waltham, MA), anhydrous methanol and a coulometric reagent was purchased from EMD (Gibbstown, NJ, USA). A Millipore water purification system with a 0.22μm filter was used for water.

3.3 Experimental

3.3.1 Differential Scanning Calorimetry (DSC)

Thermal analysis was performed via a Q1000 differential scanning calorimeter (DSC) with an auto sampler (TA Instruments, New Castle, DE) and calibrated with indium. Drug samples were weighed (3-4 mg) and placed into an aluminum hermetic pan with a pin-hole lid. A nitrogen purge of 40 ml/min was used throughout. Samples were allowed to equilibrate at 30°C for five min, followed by a heat ramp of 10°C/min up to 400°C to determine the melting point (T_M). When investigating possible pseudopolymorphs, the initial equilibration period was followed by a heat ramp of 10°C/min up to 150°C, then cooled to 30°C, and followed by a second heat ramp to 150°C. The enthalpy of the phase transition was calculated by the area under the curve for each endotherm while the entropy of the phase transition was obtained by the following equation.

$$\Delta S_x = \frac{\Delta H_x}{\Delta T_x} \qquad \text{Eqn. 3.1}$$

Where:

ΔS_x Entropy of transition

ΔH_x Enthalpy of transition

ΔT_x Transition temperature (K)

3.3.2 Thermogravimetric analysis (TGA)

Thermogravimetric analysis (TGA) was performed on a Q50 TGA (TA Instruments, New Castle, DE). Samples were weighed (3-4 mg) in aluminum pans, sealed with aluminum lids, and heated at 5°C/min up to 400°C. Weight loss as a function of temperature was analyzed and a nitrogen purge of 60 ml/min was utilized.

3.3.3 Karl Fisher Titration (KF)

Water content in different forms of MYR was determined using a TitroLine 7500 Karl Fisher titrator (SI Analytics, Germany). Samples were analytically weighed (2-3 mg), dissolved in anhydrous methanol, and transferred to the titration vessel. A blank sample of anhydrous methanol was used to baseline the system. Samples were run in duplicate.

3.3.4 X-ray powder diffraction (XRD)

X-ray powder diffraction (XRD) was conducted with a PANalytical X'Pert MPD (PANalytical Inc., Westborough, MA) system with a copper anode (Kα radiation (λ) = 1.54 Å) at 45 kV (40mA target current). High-resolution scans were conducted along the goniometer axis (θ/2θ) at a step size of ca. 0.0167°. Approximately 2700 scans were

taken between 2θ of 5.0 and 50.0. Samples were placed on a zero background plate and rotated at 0.25 rps.

3.3.5 High performance liquid chromatography (HPLC)

Reverse-phase high performance liquid chromatography (HPLC) was used to analyze drug concentrations from a variety of experimental conditions. Samples were analyzed with a Waters system consisting of a 2695 separation module, coupled with a 2487 dual absorbance detector (Waters Corporation, Milford, MA). Separation was achieved using a 150 mm x 3.9 mm Apollo C18 5.0 µm column. UV detection was conducted at 373 nm. An isocratic method developed for the detection of the flavonol quercetin (Chen-yu, 2012) was adapted for MYR analysis. A mobile phase (50:50) consisting of methanol:acetic acid (3%) with a run time of 10 min was utilized. Standards were prepared from a roughly 500 µg/ml stock solution of MYR in 100% methanol (MeOH) and ranged from 0.5-200 µg/ml. The retention time for MYR was approximately 4.5 min. Samples were run with a constant flow rate of 1 ml/min and an injection volume of 10 µl. All quantifications were based on peak area.

3.3.6 Solubility determination

Solubility values for MYR were determined by adding excess drug to scintillation vials containing 20 ml of solvent and then agitated with a rocking shaker. Samples were

collected at 30 and 60 min intervals for up to 8 hrs, and then again at 24 hrs. Additionally, dissolution studies were performed at 4, 23, 35, and 56°C. In an effort to improve solubility, so that differences in relative solubility could be distinguished, 20% ethanol (EtOH) was utilized as a cosolvent. Samples were collected at 60 min intervals for up to 8 hrs, then at 24 hrs. Sampling continued until equilibrium was reached. The solubility of MYR was also determined as a function of various cosolvents. EtOH, MeOH, glycerol (Gly), propylene glycol (PG), and polyethylene glycol 400 (PEG 400) were mixed with water (pH=5, 0.1M citrate buffer) in volume fractions of 0.05, 0.15, 0.3, and 0.5.

Prior to HPLC analysis, samples were filtered with a 0.2 μm PTFE filter. Potential adsorption of the drug to the filter membrane was investigated by comparing the difference in drug concentration of a standard solution (methanol) before and after filtration with the difference being less than 0.5%. All experimental conditions were investigated in duplicate.

3.3.7 Partitioning

A partitioning study was conducted in order to determine the apparent partition coefficient (*P*) of MYR. *1*-octanol was added to an equal volume of a 0.1M citrate buffer at pH 5. Six vials containing this mixture where kept on a shaker for 24 hrs at 23°C to reach equilibrium. Due to the low solubility of MYR an excess of drug was added to the

vials and placed back on the shaker for an additional 24 hrs. MYR was then allowed to separate into the two phases over the next 24 hrs. A portion of each phase was sampled, centrifuged, and filtered with a 0.2 µm PTFE filter. *1*-octanol phases were diluted 1:1 with ACN and both phases were analyzed by the HPLC method described above.

3.3.8 Stability Studies

3.3.8.1 Effect of pH

The effect of pH on the stability of MYR was determined using a citrate buffer in the pH range of 3-5, a phosphate buffer in the pH range of 5-8, and a borate buffer in the pH range of 8-10. Buffers were prepared to a concentration of 0.1M and pH adjusted with NaOH and HCl as needed and with NaCl to a constant ionic strength of 0.2M. Samples were prepared with 20% MeOH (V/V) as a cosolvent and a target MYR concentration of 100 µg/ml. Degradation was observed over 3 weeks at 23°C. Stability was determined in duplicate using the HPLC method described above. Shelf life (T_{90}) and half-life (T_{50}) were calculated from the degradation rate constant (κ) for each pH investigated.

3.3.8.2 Effect of oxidation

The effects of oxidation on the stability of MYR were investigated by comparing solutions containing 1.5% hydrogen peroxide (H_2O_2) and adding either 0.1% ascorbic

acid (AA), or 0.1% sodium metabisulfite (SMS) to assess the effectiveness of the antioxidants. EtOH was used as a cosolvent (20%) to enhance drug solubility and degradation was observed for 3 weeks at 23°C. Stability was determined in duplicate using the HPLC method described above. Shelf life (T_{90}) and half-life (T_{50}) were calculated from the degradation rate constant (κ) for each system.

3.3.8.3 Effect of UV irradiation

Stability was determined by exposing a solution of MYR in acetone to UVR. Samples were prepared with a target concentration of 200 µg/ml and exposed to a bank of two UVA Sun 340 sunlamps. Lamps emit UV between 295 and 390 nm which include both UVA and UVB wavelengths. Samples were exposed for 82 min for a total dose of 470 mJ/cm^2. Doses stated represent the UVB portion of the lamp output. Stability was determined in duplicate using the HPLC method described above. Shelf life (T_{90}) and half-life (T_{50}) were calculated from the degradation rate constant (κ).

3.4 Results and discussion

3.4.1 Differential Scanning Calorimetry (DSC)

DSC curves for both MYR I and MYR II can be seen in Figure 3.1 and Figure 3.2, respectively.

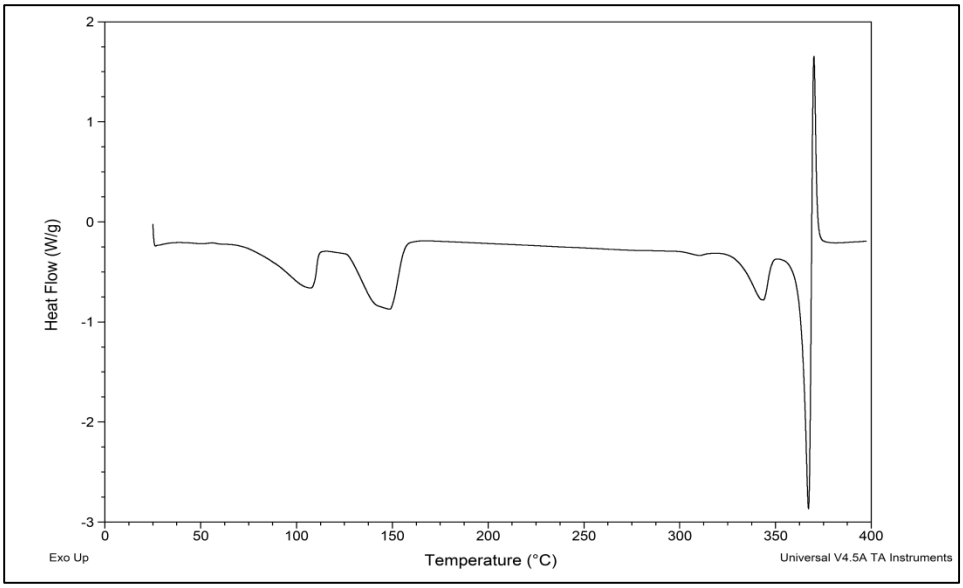

Figure 3.1 DSC profile of MYR I.

The DSC profile for MYR I exhibited a total of four endotherms (down) and one exotherm (up). The fourth endotherm, onset temperature of 363°C, was deemed to be the melting point, while the endotherm just prior is believed to an indication of a phase-transition. The two sequential endotherms during the early stages of the thermal cycle (onset temperature of 81°C, 128°C) were interpreted to represent solvent loss (water).

Similarly, the MYR II profile also exhibited four endotherms with an onset melting temperature of 361°C. However, solvent loss (dehydration) is represented by a single endotherm (onset temperature of 50°C).

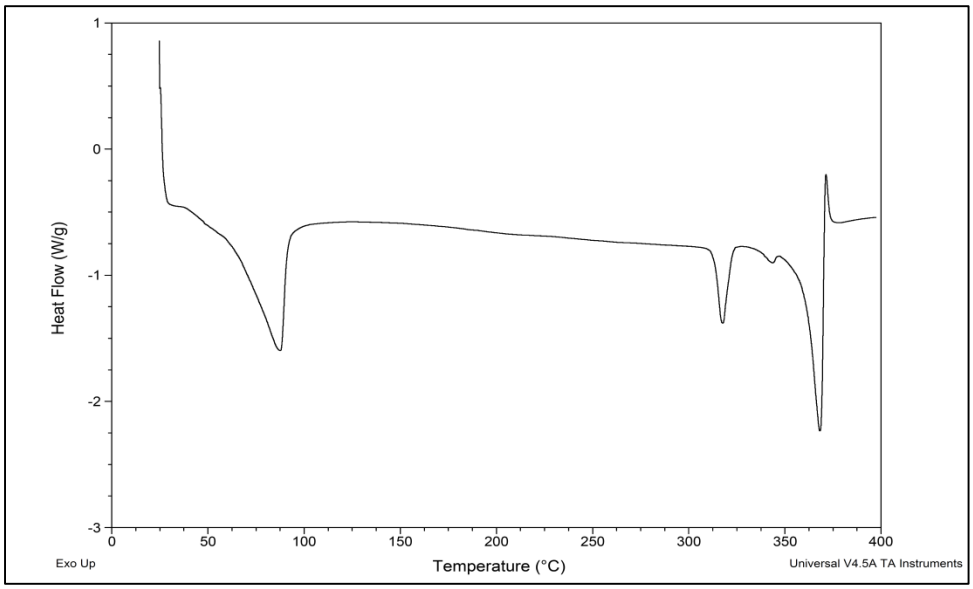

Figure 3.2 DSC profile of MYR II.

The differences between the DSC profiles, particularly the different onset dehydration temperatures, suggests a difference between the two drug lots that is due to different hydrate crystal structures. For example, the lower dehydration temperature of MYR II, along with the broad endotherm profile, is characteristic of a channel binding hydrate (Brittain, 2009). In comparison, the sharper endotherms of MYR I are more typical of hydrates that contain isolated binding sites (Brittain, 2009). Entropies of transition (ΔS_x) were calculated from endotherm onset temperatures (T_D) and the corresponding enthalpies of transition. These values can be seen in Table 3.1. Since both MYR hydrates possess a unique DSC profile, potential conversion between crystal forms was investigated. Following a seven day period, excess solid was sampled from a solubility study (23°C) and DSC profiles indicated that neither MYR IA nor MYR IIA had reverted back to a hydrated state nor did either hydrate convert to another form.

	T_D-1 (°C)	ΔS_D-1 (cal/K*mol)	T_D-2 (°C)	ΔS_D-2 (cal/K*mol)	T_M (°C)	ΔS_M (cal/K*mol)
MYR I	81	12.7	128	17.4	363	11.0
MYR II	50	37.7	-	-	361	10.2

Table 3.1 Transition temperature and calculated entropy for two forms of MYR.

With the apparent presence of a hydrate, an attempt to de-solvate the crystal was made. A quantity of MYR I and MYR II (3-5 mg) was run in a DSC cycle that included an initial heat ramp of 150°C, followed by a cool down to 40°C, and finished with a second heat ramp to 150°C. Removal of any potential water was confirmed by heating the same sample up to 400°C. An example can be seen in Figure 3.3 which illustrates the dehydration of MYR I, the resulting crystal referred to as MYR IA.

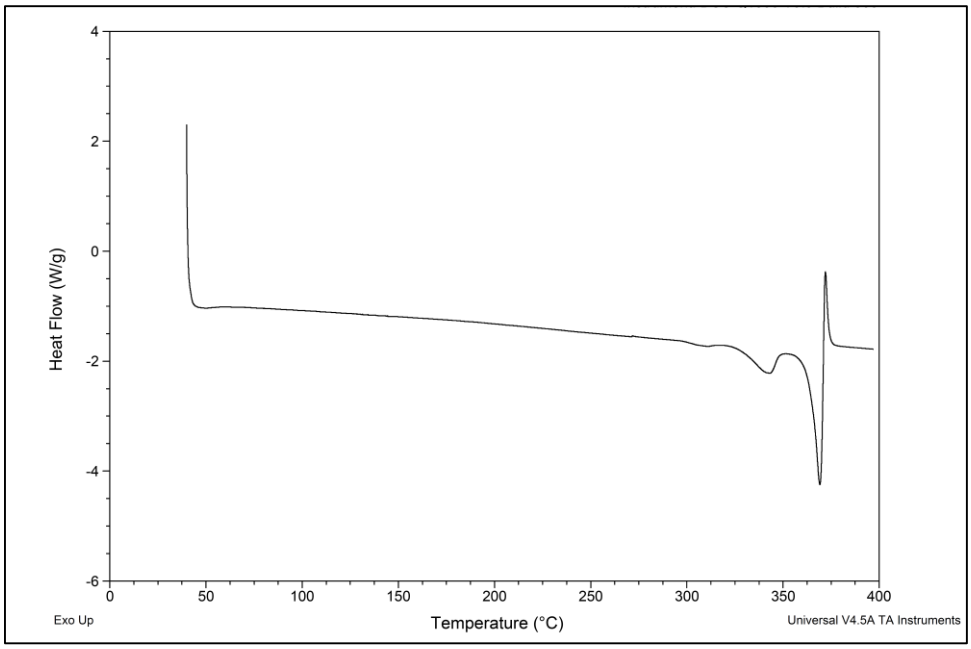

Figure 3.3 DSC profile of MYR IA (desolvate).

From the profile, one can see the dehydration endotherms are no longer present. However, features that are seen in the MYR I profile are, such as onset melting point (≈363°C) and entropy of melting ($\Delta S_m \approx$ 11.0 cal/k*mol).

3.4.2 Thermogravimetric analysis (TGA)

TGA studies were performed on both MYR I and MYR II and those profiles can be seen in Figure 3.4 and Figure 3.5, respectively. Weight loss as a function of temperature was analyzed to determine water loss from the crystal. Weight loss attributed to dehydration was used to help determine the stoichiometry of water:drug molecules present.

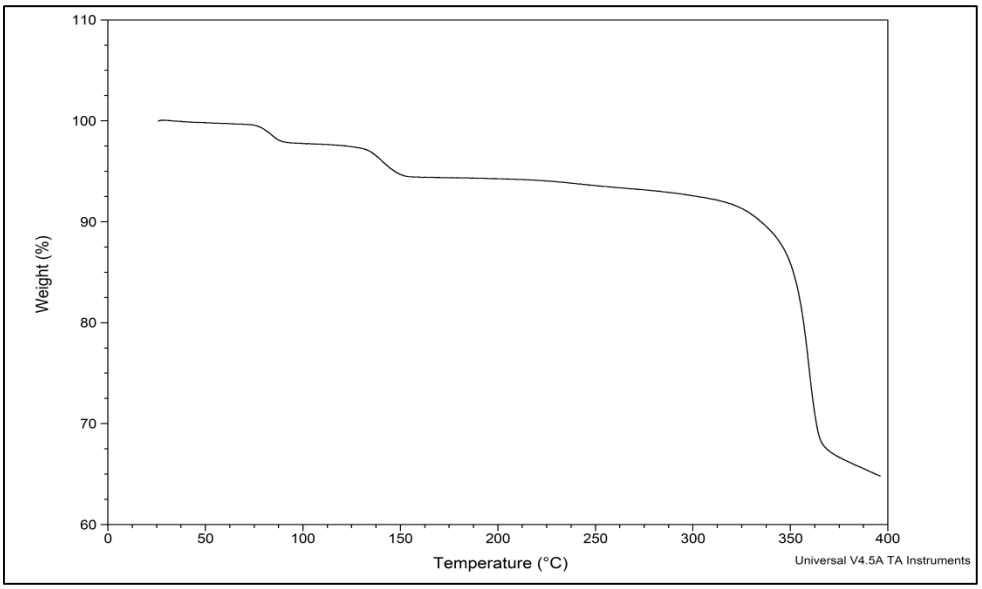

Figure 3.4 TGA profile of MYR I.

The TGA for MYR I showed two visible plateaus with onset temperatures similar to its DSC profile (≈ 80°C and 125°C). Total weight loss attributed to dehydration was estimated at 5.6% which represents roughly 1.04 moles of water per mole of MYR. Again, the high dehydration onset temperature is characteristic of an isolated binding site hydrate (Brittain, 2009) and in this instance strong confidence can be placed in labeling MYR I as a monohydrate.

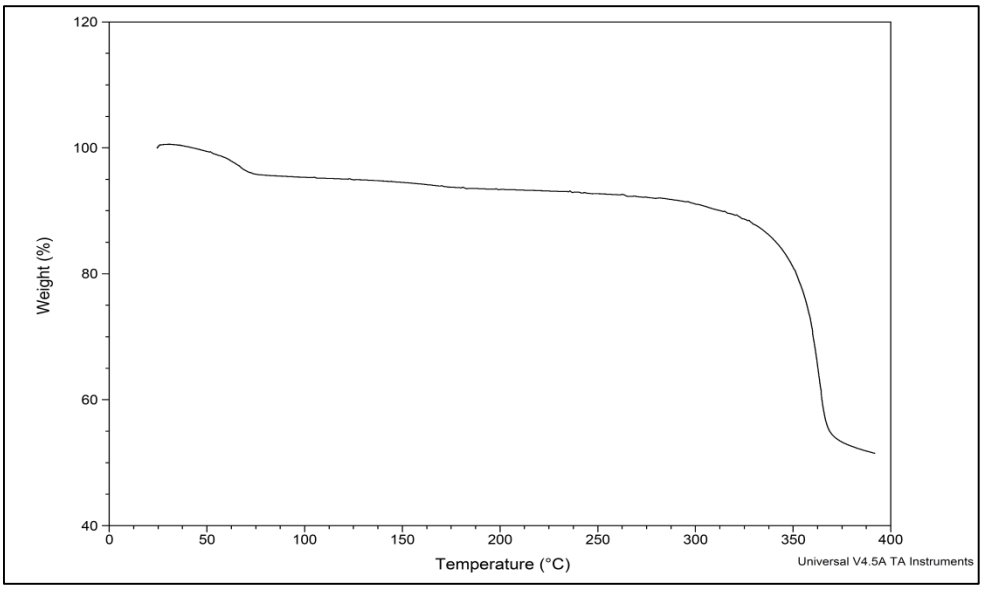

Figure 3.5 TGA profile of MYR II.

In comparison, the profile for MYR II showed one plateau beginning around 50°C that resulted in 5.2% weight loss which corresponds to 0.97 moles of water per mole of MYR. Again, the low onset dehydration temperature is typical of a channel hydrate (Brittain, 2009). The differences between MYR I and MYR II thermal profiles strongly suggest different water binding sites for the two drug lots. Following these results a quantity of both MYR lots were dehydrated for future studies. This was achieved by heating the sample to 150°C in the TGA, holding the temperature for 30 min, and verifying the absence of water with the DSC. Dehydrated forms are referred to as MYR IA and MYR IIA, respectively.

3.4.3 Karl Fisher Titration (KF)

Karl Fisher titration confirmed the presence of water in the starting material for both MYR I and MYR II. The average water content for MYR I was 4.9%, converting to an estimated 0.87 moles of water per mole of MYR. By comparison, the average water content for MYR II was 11.7%, resulting in an estimated 2.07 moles of water per mole of MYR, which is twice of that found from the TGA studies.

3.4.4 X-ray powder diffraction (XRD)

Four forms of MYR were characterized by X-ray powder diffraction (Figure 3.6).

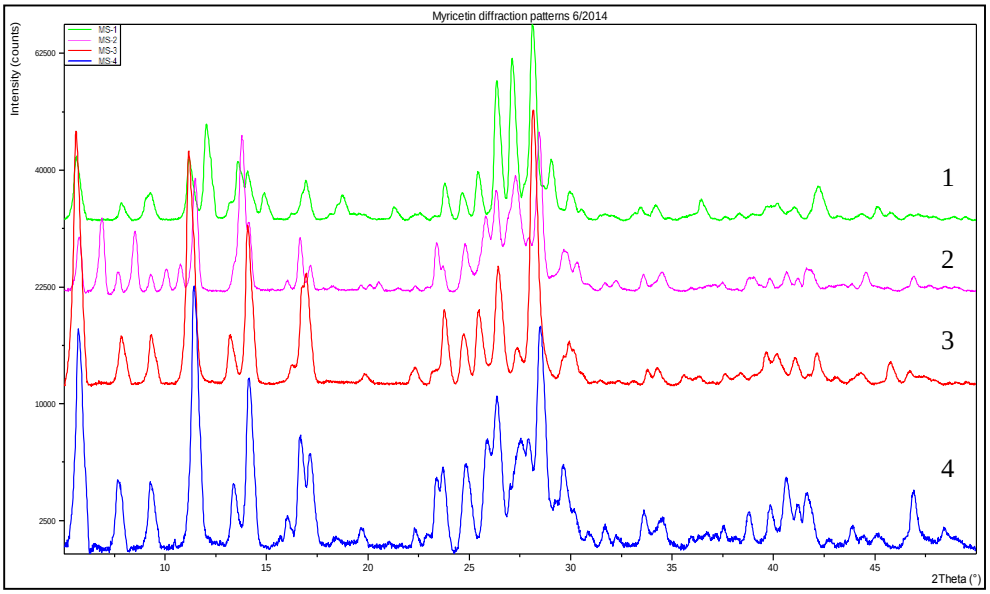

Figure 3.6 XRD Overlay: MYR I (1) MYR IA (2) MYR II (3) MYR IIA (4).

Differences between all four diffraction patterns were seen across the full range of 2θ. Differences in the diffraction patterns of the starting materials (patterns 1, 3) confirm a different crystal structure for each hydrate. Comparing these patterns showed differences in diffraction, for example between 10-15, 25-30 and 40-45 2θ. Similarly, when comparing MYR I and MYR IA (patterns 1, 2), substantial changes were seen in the diffraction patterns following dehydration, indicating a different crystal structure for the anhydrous form. Comparing these patterns, differences in diffraction was seen between 5-20, 25-30 and 40-45 2θ. In the case of MYR II and MYR IIA (patterns 3, 4) different diffraction patterns were also seen particularly between 25-30 2θ, however, the differences are less distinct, suggesting that the two crystal forms share some similar structural attributes. The lack of disparity between MYR II and MYR IIA suggest the presence of an apparent isomorphic desolvate (Stephenson, 1998). An isomorphic desolvate is defined as a desolvate that retains the three-dimensional order of the original crystal form (Stephenson, 1998).

3.4.5 Solubility Determination

3.4.5.1 Aqueous Solubility

Aqueous solubility for MYR was determined at 23°C. The dissolution profiles of the four forms of MYR can be seen in Figures 3.7 and 3.8, respectively. From Figure 3.7, a difference in solubility between MYR I and MYR IA can be seen. The dissolution

profile of MYR I had a maximum solubility of 1.08 µg/ml and remained relatively close to 1 µg/ml for the first 8 hrs until reaching an apparent equilibrium value of 0.48 µg/ml after 24 hrs. Comparatively, the apparent solubility of MYR IA reached a maximum of 5.04 µg/ml but began to decline more rapidly, leveling off around 3.21 µg/ml after 24 hrs.

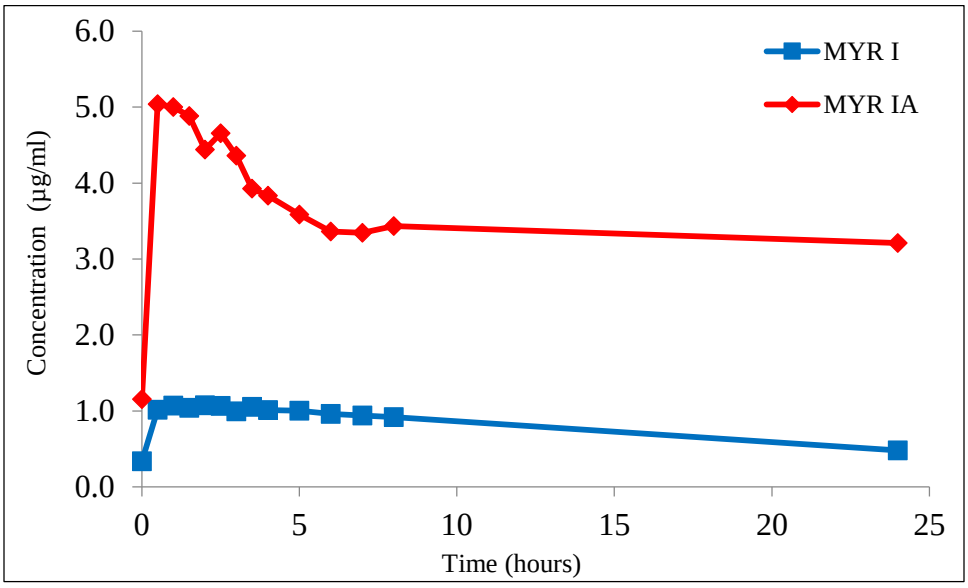

Figure 3.7 Dissolution profile of MYR I and MYR IA in water (23°C).

From Figure 3.8, the dissolution profile of MYR II and MYR IIA indicate that the relative solubility difference between the two forms is not substantial, when compared to the relative difference between form I and IA. Solubility for both MYR II and MYR IIA had an initial value under 1 µg/ml (0.64 µg/ml and 0.72 µg/ml respectively) and after 24 hrs apparent equilibrium values were similar to their initial values (0.61 µg/ml and 0.72 µg/ml).

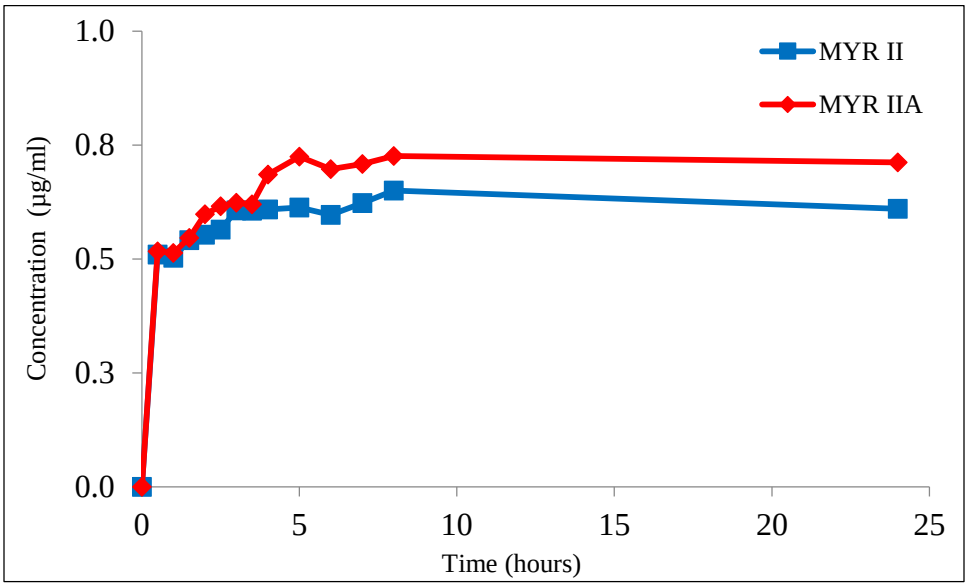

Figure 3.8 Dissolution profile of MYR II and MYR IIA in water (23°C).

From both sets of profiles, the solubility of MYR appears to be descending, albeit only slightly in the case of MYR II. As such, it is unclear if 24 hrs represents equilibrium for MYR. An effort was made to collect additional data (48 hrs), however the solubility values were below the limit of detection for this particular HPLC method. If equilibrium had been reached, this study suggests that MYR I is the more stable crystal form resulting from its lower solubility. Since both MYR I and MYR II can be categorized as highly insoluble, further studies comparing the two were done by altering parameters to enhance the solubility. This includes the addition of a cosolvent to the system and evaluating solubility at different temperatures.

3.4.5.2 Effect of temperature

Dissolution studies were performed at 4, 23, 35, and 56°C. In an effort to improve solubility so that differences in relative solubility could be distinguished, 20% ethanol (EtOH) was utilized as a cosolvent. The dissolution profiles comparing the solubility of MYR I and MYR II at 23 and 35°C can be seen in Figures 3.9 and 3.10, respectively.

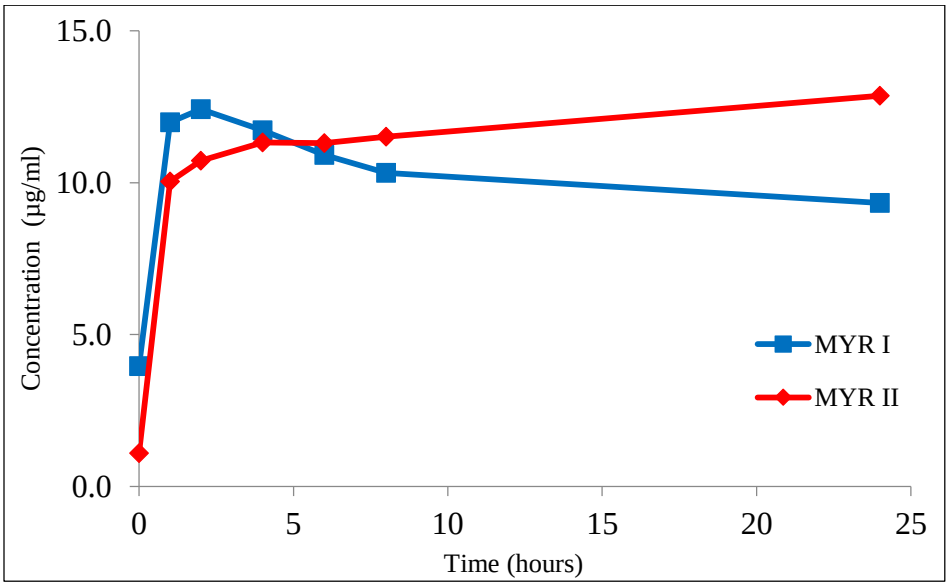

Figure 3.9 Dissolution profile of MYR I and MYR II in 20% EtOH (23°C).

The dissolution profile from Figure 3.9 (20% EtOH, 23°C) shows that MYR I had an initial solubility of 12.42 µg/ml that began to decline after 2 hrs reaching an apparent equilibrium solubility of 9.33 µg/ml after 24 hrs. Comparatively, MYR II gradually reached its apparent equilibrium solubility of 12.86 µg/ml after 24 hrs. This study suggests that MYR I is more stable at 23°C due to its lower solubility after 24 hrs.

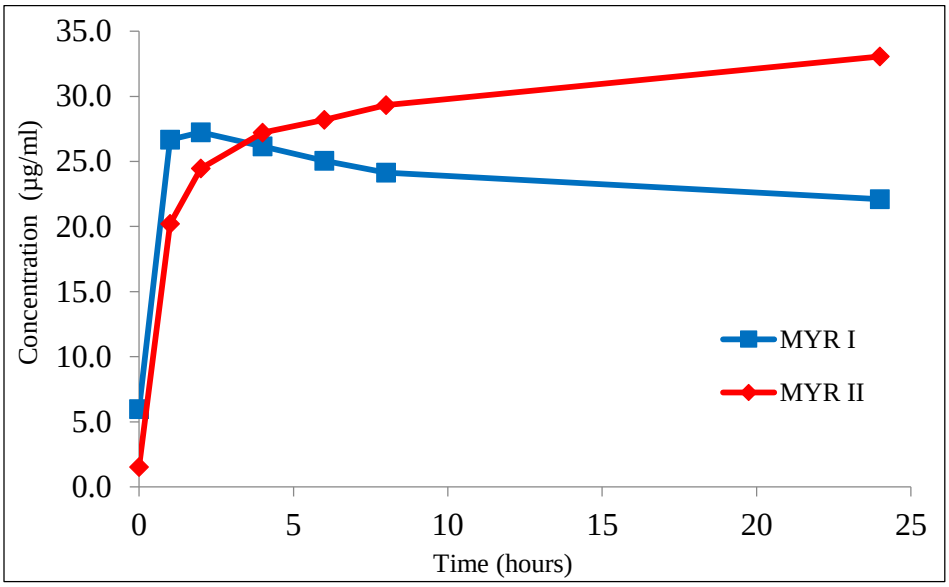

Figure 3.10 Dissolution profile of MYR I and MYR II in 20% EtOH (35°C).

The dissolution profile from Figure 3.10 (20% EtOH, 35°C) shows that MYR I had an initial solubility of 27.23 µg/ml which began to decline after 2 hrs reaching an apparent equilibrium solubility of 22.09 µg/ml after 24 hrs. Comparatively, MYR II gradually reached its apparent equilibrium solubility of 33.06 µg/ml after 24 hrs. This study suggests that MYR I is more stable at 35°C due to its lower solubility after 24 hrs. Interestingly, at both temperatures (23°C and 35°C) MYR I had a faster dissolution rate than MYR II, but over time MYR II solubility would exceed that of MYR I. The results from 4°C and 56°C can be seen in the Arrhenius plot below in Figure 3.11.

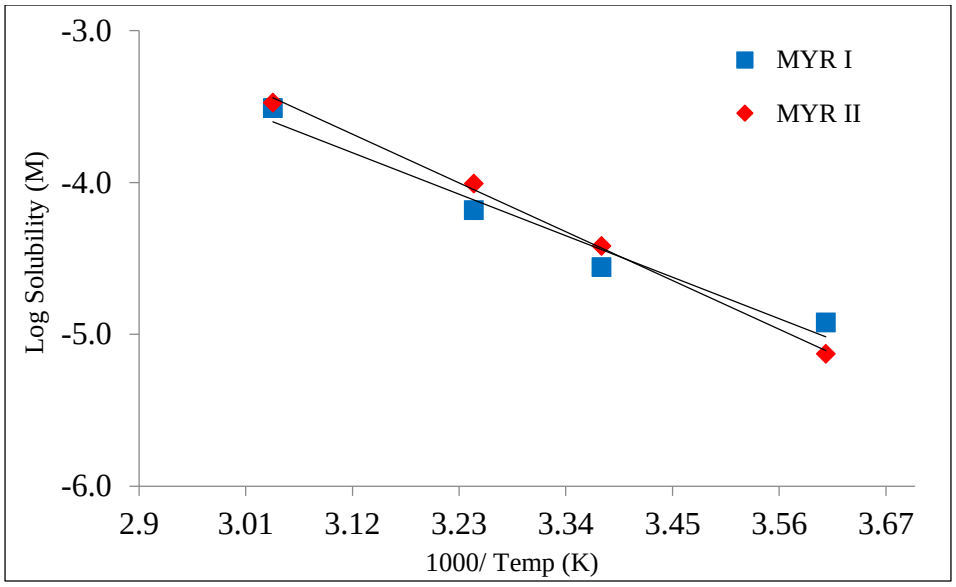

Figure 3.11 Arrhenius plot of MYR I and MYR II in 20% EtOH .

In Figure 3.11, logarithm solubility values (Mol/L) are plotted versus the inverse of temperature (K) and results indicate an apparent enantiotropic-like relationship over the experimental temperature range. The MYR I series has a slope of -2.48 and a calculated enthalpy of solution ($\Delta H_{solution}$) of 20.18 kJ/mol. Similarly, MYR II has a slope of -2.92 and a $\Delta H_{solution}$ of 23.72 kJ/mol.

3.4.5.3 Cosolvent Solubility

Solubility of MYR was determined at pH 5 for several commonly used cosolvents, EtOH, MeOH, Gly, PG and PEG 400. Figure 3.12 shows the effect of cosolvent concentration, as a function of the volume fraction, on the solubility of MYR.

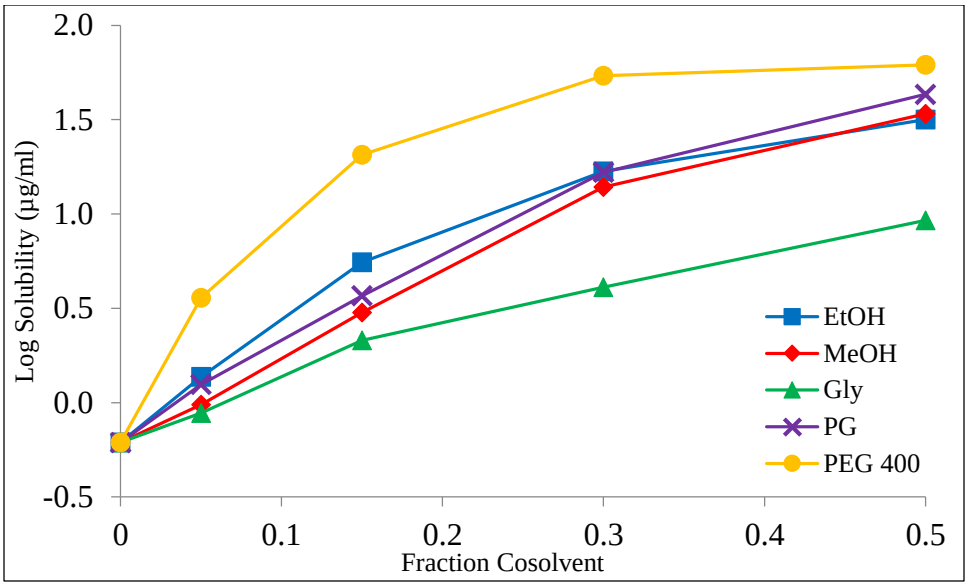

Figure 3.12 Effect of fractional cosolvent on MYR solubility (pH5, 23°C).

A general log-linear increase in solubility can be seen for each cosolvent, however there are differences in curvature. With 0.5 cosolvent the highest increase in solubility was achieved with PEG 400 (72.79 µg/ml) while the lowest solubility was seen with Gly (10.11 µg/ml). The remaining three cosolvents had nearly identical results. While there was a substantial increase in solubility with PEG 400, over 100x, it still represents a poorly soluble solution. Table 3.2 presents the initial solubilization slopes (σ) obtained for each cosolvent as well as the solubility determined with 0.5 cosolvent.

	EtOH	**MeOH**	**Gly**	**PG**	**PEG 400**
Solubilization Slope (σ)	5.16	4.64	2.41	5.04	9.74
Solubility (µg/ml)	49.37	48.51	10.11	54.72	72.79

Table 3.2 MYR solubility (pH 5, 23°C) with 0.5 cosolvent.

3.4.6 Partitioning Study

An average of six measurements of MYR added to 1:1 *1*-octanol:water was used to determine the partition coefficient. The concentration of MYR in the *1*-octanol phase was determined to be 870 times higher than in the aqueous phase. The resulting oil/water partition coefficient (log P) is therefore 2.94. This value is in agreement with the 1:10 and 1:5 *n*-octanol:water data reported (Yao, 2014).

3.4.7 Stability Studies

3.4.7.1 Effect of pH

Drug stability can be affected by different pHs, catalyzed by either hydrogen ions or hydroxide ions and in some cases both. Stability of MYR was determined at eight different pHs ranging from 3 to 10 and utilizing different 0.1M buffers (citrate, phosphate, and borate) at 23°C and a constant ionic strength of 0.2M. In two instances, at pH 5 and 8, different ion species were used to compare their effect on degradation. From the kinetic rate profiles (data not shown), it is evident that MYR undergoes apparent first-order kinetics in the pH conditions investigated. The degradation rate constants (κ) were calculated from the slope of the log-linear best fit regression line by the following equation.

$$\kappa = -Slope \times 2.303 \qquad \text{Eqn. 3.2}$$

Rate constants were used to plot a pH-rate profile (Figure 3.13) for MYR that indicates that MYR undergoes base-catalyzed degradation. Interestingly, the slope from pH 5 (citrate) to pH 10 (borate) is 1.5 with an R^2= 0.99, potentially indicating that in addition to base catalysis there may be other mechanism of degradation occurring.

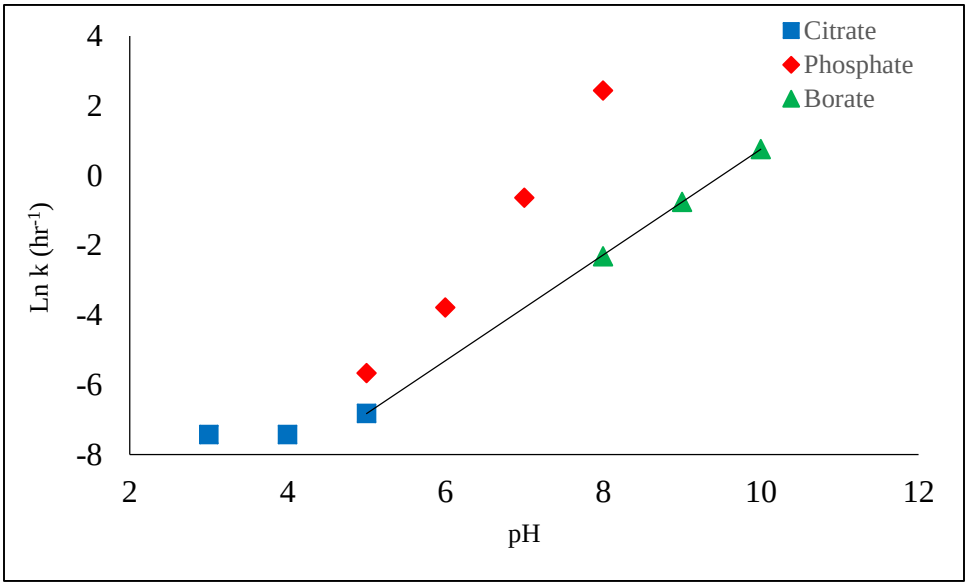

Figure 3.13 MYR pH rate profile, natural logarithm of degradation rate constant (κ) versus pH (23°C).

From the degradation rate constant, half-life (T_{50}) and shelf life (T_{90}), defined as the time at which 10% of the drug has degraded, can be calculated. These values can be obtained by Equation 3.3 and 3.4, respectively. A summary of the data can be seen in Table 3.3.

$$\frac{0.693}{\kappa} = T_{50} \qquad \text{Eqn. 3.3}$$

$$\frac{0.105}{\kappa} = T_{90} \qquad \text{Eqn. 3.4}$$

pH	κ (per hr)	$\mathbf{T_{50}}$(hrs)	$\mathbf{T_{90}}$(hrs)
3 (Citrate)	0.0006	1155	175
4 (Citrate)	0.0006	1155	175
5 (Citrate)	0.001	630	95.5
5 (Phosphate)	0.004	198	30
6 (Phosphate)	0.02	30.1	4.6
7 (Phosphate)	0.5	1.3	0.2
8 (Phosphate)	11.6	0.1	0.01
8 (Borate)	0.1	7.0	1.1
9 (Borate)	0.5	1.5	0.2
10 (Borate)	2.2	0.3	0.1

Table 3.3 Degradation rate constant, half-life, and shelf life for MYR at various pHs.

From the data it is evident that the stability of MYR is highly dependent on pH. In fact, stability varied nearly 10 log units between the maximum and minimum rate of degradation. The most stable condition was pH 3 citrate buffer (T_{50}=1155 hrs) while the

least stable was pH 8 phosphate buffer (T_{50}=0.1 hr). When comparing buffer species, accelerated degradation was seen with phosphate buffer, as evidenced by pH 8 borate buffer having a T_{50}=7.0 hrs. Likewise, at pH 5, the citrate samples had a T_{50}=630 hrs, while phosphate had a T_{50}=198 hrs. No pH change was noted in any of the samples over the course of the study.

3.4.7.2 Effect of Oxidation

Accelerated oxidation can be achieved with the aid of peroxides. In low concentrations, hydrogen peroxide will produce primary oxidative degradation products and stability can be analyzed over time. From the kinetic rate profile (Figure 3.14), it appears that MYR undergoes apparent first-order kinetics.

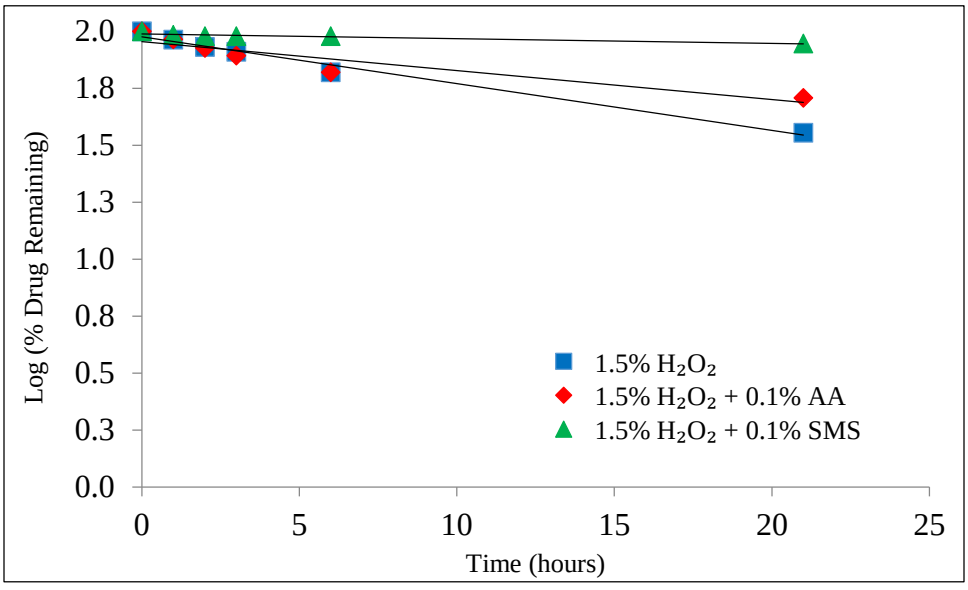

Figure 3.14 Effect of oxidation (20% EtOH, 23°C).

MYR appears to be fairly labile in a 1.5% H_2O_2 solution (T_{50}=14.6 days). A moderate improvement in stability was seen when adding 0.1% of the anti-oxidant ascorbic acid (AA) (T_{50}=23.7 days) whereas a greater improvement was seen with the addition of 0.1% sodium metabisulfite (SMS) (T_{50}=143.5 days).

3.4.7.3 Effect of UV Irradiation

Exposure to UVA and UVB has been shown to cause DNA damage, erythema, immunosuppression, and eventually, skin cancer (Melnikova, 2005; Setlow, 1974). A solution of MYR in acetone (≈ 200 μg/ml) was dosed with 470 mJ/cm^2 of UVR (295-390nm). Following exposure, MYR retained approximately 87% of the initial drug concentration.

3.5 Conclusions

Solid state characterization of MYR indicate that it can exist in two hydrated states, which had been previously unreported. Studies suggest that these two crystal forms possess different binding properties for the attached water molecules. DSC and TGA analysis support that an isolated binding site exists for MYR I in the form of a monohydrate, while MYR II analysis suggests channel hydrate binding also in the form of a monohydrate. XRD patterns confirmed differences in crystal structure between all four crystal forms (both starting materials and both anhydrous forms). The pattern similarities between MYR II and MYR IIA suggest that MYR IIA is possibly an isomorphic desolvate. Following a seven day solubility study, DSC analysis of excess solid material revealed that neither MYR IA nor MYR IIA had reverted back to a hydrated state nor did either hydrate convert to another form. Relative differences in solubility were difficult to interpret in pure water but it was evident that both forms are highly insoluble. Improved solubility was achieved using a variety of cosolvents, with the greatest effect seen in PEG 400. With the aid of the cosolvent ethanol, solubility studies confirmed that MYR I is the more stable form at 23 and 35°C.

It has been shown that MYR undergoes rapid apparent first-order degradation under basic pH conditions, and that degradation can be influenced by buffer species with accelerated degradation seen in phosphate buffer. Apparent first-order degradation was also seen when MYR was exposed to an oxidizing solution. Improved stability was

achieved after introducing 0.1% antioxidants to the solution, with the greatest improvement seen with sodium metabisulfite. Following a dose of UVR, MYR was found to have good stability, which is a consideration for topical applications. Finally, a partitioning study indicated that MYR possess a log P (2.94). This investigation provided evidence that both the solid-state properties and solution stability of MYR are important to consider when developing future formulations.

CHAPTER IV: HYDRATES AND SOLUBILITY

4.1 Introduction to Hydrates

Many organic compounds can crystallize into different crystal arrangements; these arrangements are known as polymorphs. While their chemical compositions are the same, the differences in crystal structure can influence physical and chemical properties such as free energy, chemical stability, dissolution rate, apparent solubility, and potentially bioavailability. With some crystalline solids, solvent molecules may become integrated within the crystal lattice. These adducts are called solvates, or hydrates when the solvent is water. The term pseudopolymorph is used to describe this difference in crystal structure based on the inclusion of a solvent. With hydrates, water molecules align themselves within the crystal lattice, typically hydrogen bonding with the drug molecule.

The addition of the water molecule(s) in the crystal lattice alters the physical structure and properties of the drug substance including changes to the dimensions, shape, symmetry, and capacity of the unit cell. These changes lead to differences in pharmaceutical properties such as solubility and chemical stability (Grant, 1995). Notably, the hydrate of a drug substance usually has a lower aqueous solubility. A change in drug solubility, specifically a decrease in solubility, could limit the drug concentration of the formulation, possibly resulting in insufficient bioavailability.

It has been estimated that one-third of active pharmaceutical substances are capable of forming a hydrate (Qu, 2011). From a pharmaceutical perspective, an unexpected phase transition from anhydrous to the hydrate form could lead to differences in product performance and alter the way a drug candidate is processed and formulated (Brittain, 2009). An example of this would be metronidazole benzoate and its monohydrate. The anhydrous form was formulated in a suspension and stored at room temperature. However, the monohydrate is the thermodynamically stable form below 38°C (Hoelgaard, 1983). As a result of the phase transition, particle size increased which led to physical instability. Additional examples demonstrating the significance of hydrate systems can be found in the literature and include; ampicillin anhydrate having higher blood serum levels in humans subjects before transitioning to the stable trihydrate (Poole, 1968), theophylline anhydrate having more than double the apparent solubility over its monohydrate at 25°C (Rodriguez-Hornedo, 1992) and the complications of measuring dissolution rate and solubility of carbamazepine anhydrous due to the rapid transition (1hr) to the dihydrate (Young, 1991).

The estimation of solubility for a drug or drug candidate is an important aspect to the drug development process for both academic and industrial research. As such, the development of models to predict solute solubility in both aqueous and organic solvents, as well as the effects that cosolvent, surfactant, and pH have on solubility have been investigated for decades. Computational models based on substructure components, solvation interactions, and lipophilicity can be found throughout the literature.

Additionally, many review articles are available that discuss the advantages and disadvantages of different prediction models (Faller, 2007). Most of these solubility estimation methods either assume the most stable anhydrous crystal, or don't address the impact of different crystal forms. A previous model has been developed to predict the solubility ratio of polymorphs (Mao, 2005). However, there are no models that take into consideration additional energies present with hydrates, nor how those energies would affect the overall solubility.

4.2 Solubility of Anhydrous Crystalline Solutes

The solubility of a solid solute is related to the energy necessary to break-up the crystal and the mixing with a solvent. The influence of the crystal term can be derived as a function of the melting point; however the mixing term is only considered for non-ideal conditions, and is dependent on the chemical structure of the solute and how it interacts with the solvent. For aqueous conditions, the mixing interaction is often accounted for by the solute's partition coefficient (Kow or P).

When evaluating the solubility of a solid solute it is necessary to consider the energetics of the crystal. The influence of the crystal on solubility can be related to how much energy it takes to convert the crystal into a hypothetical supercooled liquid (HSL) at a given temperature. Kirchoff's law states that the energy of an irreversible process is equal to the energy of a series of reversible processes between the same end points

(Kirchoff, 1860). As such, the enthalpy of melting at temperature, T (converting the solid to HSL), can be described by the sum of the enthalpies of the following processes; heating the solid to its melting point, melting the solid at is melting point, and cooling the liquid back down to temperature, T. This process is illustrated (1→4) in Figure 4.1.

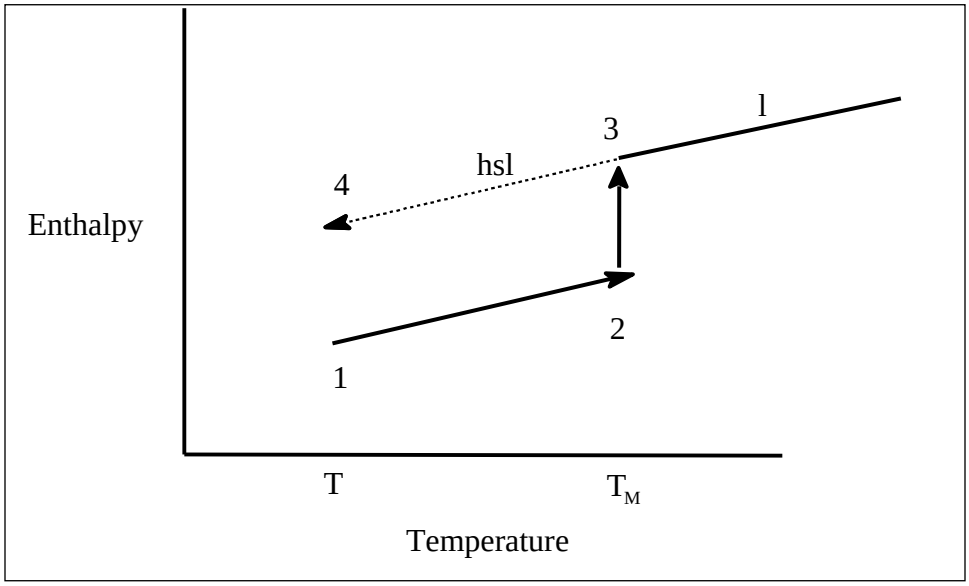

Figure 4.1 Thermodynamic process of a solid solute going to a HSL at temperature T.

The effect of the crystalline contribution on the ideal solubility of a solid solute can be determined from its solid-state properties via equation 4.1 (Jain and Yalkowsky, 2001).

$$RlnX_u^{ideal} = -\Delta H_m \ \frac{(T_m - T)}{T_m T} + \Delta Cp_m \ \frac{(T_m - T)}{T_m T} - \Delta Cp_m \ ln\frac{T_m}{T} \qquad \text{Eqn. 4.1}$$

Where X_u, ΔH_m, T_m, and R correspond to the mole fraction solubility, heat of melting, melting point of the solid, and the gas constant respectively. ΔCp_m corresponds to the difference in heat capacity between the solute's solid and liquid phases. Due to the opposing signs of each of the heat capacity terms (second and third term of Equation. 4.1), a reasonable approximation can be made to disregard the ΔCp_m term entirely as it often results in a small impact on the overall expression (especially with lower melting compounds) (Yalkowsky, 1992). Although this interpretation does fit most samples, it has been reported that in instances of increased molecular flexibility, ΔCp_m is better approximated by using the value for the entropy of melting (ΔS_m) (Neau, 1990). However, utilizing the assumption that ΔCp_m is equal to zero, and recalling that at the melting point the Gibbs free energy (ΔG) is equal to zero so that $\Delta H = T\Delta S$, equation 4.1 can be rearranged to Equation 4.2 or Equation 4.3.

$$lnX_u^{ideal} = -\Delta S_m \ \frac{(T_m - T)}{RT} \qquad \text{Eqn. 4.2}$$

OR

$$logX_u^{ideal} = -\Delta S_m \ \frac{(T_m - T)}{2.303RT} \qquad \text{Eqn. 4.3}$$

where ΔS_m corresponds to the entropy of melting.

By applying Walden's rule (Walden, 1908) which states that the ΔS_m of coal tar derivatives can be consistently approximated at 13.5 cal/K*mol, and setting the equation

to be evaluated at room temperature (°C), a convenient and efficient model (Equation. 4.4) was introduced to describe the anhydrous crystal contribution to the ideal solubility of non-electrolytes (Jain and Yalkowsky, 2001).

$$logX_u^{ideal} \approx -0.01(T_M - 25) \quad \text{Eqn. 4.4}$$

To account for the deviations from ideality the previous equations need to consider the mixing term which is dependent on the chemical structure of the solute and the activity coefficient of that solute with the non-ideal solvent, in this case, water. For liquids, the logarithm of the octanol-water partition coefficient (log Kow) can be used to account for the activity coefficient. The Kow can be estimated as the ratio of the solubility of the solute in octanol divided by the solubility in water if there is no self-association of the solute in either phase (Jain and Yalkowsky, 2001).

$$K_{ow} = \frac{S_o}{S_w} \quad \text{Eqn. 4.5}$$

$$logS_w = logS_o - K_{ow} \quad \text{Eqn. 4.6}$$

Because pure octanol contains 6.3 moles/liter a completely miscible solute would have a solubility of at least half. By taking the logarithm of 3.15 the solubility of a liquid

solute that is completely miscible with octanol can be approximated as X_u=0.5 and equation 4.6 can be arranged to equation 4.7 (Jain and Yalkowsky, 2001).

$$logS_w = 0.5 - K_{ow} \quad \text{Eqn. 4.7}$$

By combining equations (4.4) and (4.7), Yalkowsky derives the general solubility equation (GSE) for estimating the aqueous solubility (Molar) of an organic nonelectrolyte solute.

$$logS_w = 0.5 - K_{ow} - 0.01(T_M - 25) \quad \text{Eqn. 4.8}$$

4.3 Specific Aims

Estimation of crystalline solute solubility is well established throughout the literature, however, it is typically the anhydrous form that is being considered with these models. As such, there is a consistent tendency of over prediction of hydrate solubility. This can be problematic when considering that the meta-stable anhydrous form has been shown to be 2x, 3x, and even 22x more soluble then its hydrate (Pudipeddi, 2005). Therefore, the aim of this study is to describe a mathematical model based on the ideal solubility equation, which reasonably estimates the solubility of a hydrate. To develop this model the dehydration energetics of the solute needs to be considered. If successful, this model will lend itself to the appreciation of the solubility differences that can exist

between hydrate and anhydrous drug forms. Current estimation models tend to over-predict hydrate solubility which can lead to unexpected results including poor, or even unexpected, product performance. By improving the accuracy of solubility estimation, drug development studies involving hydrates can be designed accordingly.

The purpose of this study is to:

- Investigate the solid-state properties of hydrates
- Investigate the solubility of hydrates
- To develop a mathematical model to estimate the solubility of a hydrate based on thermodynamic properties which, if unknown, can be acquired from differential scanning calorimetry
- To evaluate and validate the mathematical estimates of hydrate solubility with both experimental and literature data
- To understand how variance in dehydration temperature affects the predicted solubility values when compared to experimental

CHAPTER V: HYDRATE SOLUBILITY ESTIMATION

5.1 Hypothesis

Based on the ideal solubility equation (Equation 4.1), a mathematical model to estimate the solubility of hydrates is described below. This model aims to account for the dehydration energetics of the solute as it transitions from hydrate to anhydrous prior to melting and conversion to a hypothetical super-cooled liquid (HSL) (Figure 5.1).

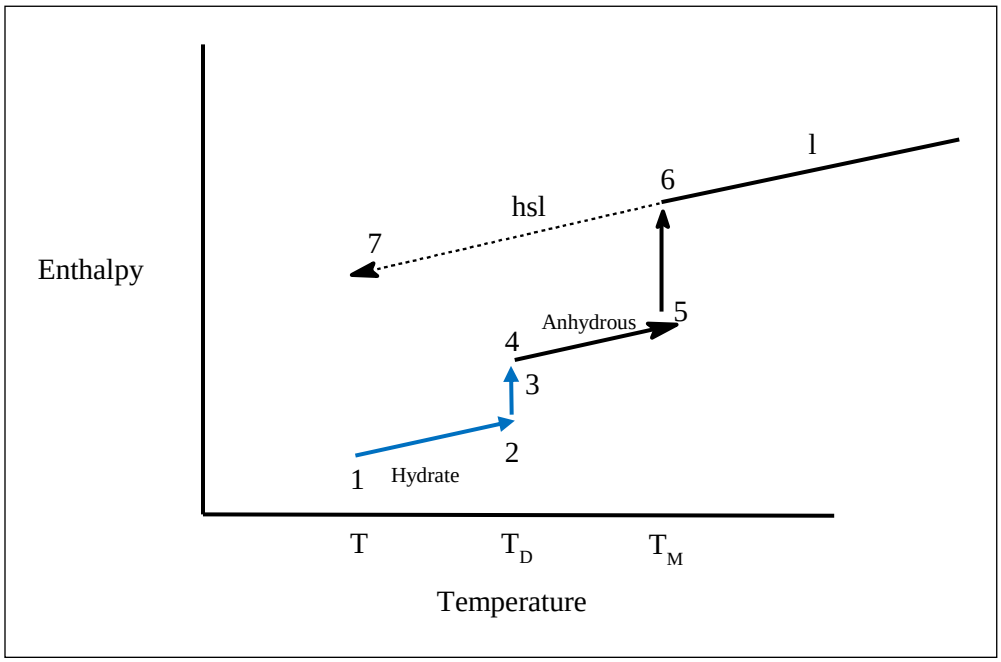

Figure 5.1 Thermodynamic process of a hydrate solid solute to a HSL at temperature T.

Where 1→4 represents the thermodynamic cycle of the hydrate solid to anhydrous solid and 4→7 represents the thermodynamic cycle of anhydrous solid to a HSL that was shown in Figure 4.1. Taking into consideration this extension of the ideal solubility theory, the hypothesis of this model is that the ideal mole fraction solubility for a hydrate is estimated by both the energy necessary to break up the crystal (melting) and the energy of transition from hydrate to anhydrous (dehydration). Furthermore, similar to the entropy of melting (ΔS_M) being estimated by 13.5 cal/K*mol, it is assumed that the entropy of dehydration (ΔS_D) is approximated by the entropy of vaporization for water; ΔS_D= 26 cal/K*mol. This model is described by equation 5.1.

$$logX_u^{ideal} = -\Delta S_m \frac{(T_m - T)}{2.303RT} - \Delta S_D \frac{(T_D - T)}{2.303RT} \quad \text{Eqn. 5.1}$$

For non-ideal conditions solubility is influenced by the activity coefficient and for aqueous systems this affect is accounted for by the partition coefficient of the solute (log P), giving Equation 5.2.

$$logX_u = -\Delta S_m \frac{(T_m - T)}{2.303RT} - \Delta S_D \frac{(T_D - T)}{2.303RT} - log\ P \quad \text{Eqn. 5.2}$$

5.2 Materials

Myricetin (MYR) monohydrate, monobasic potassium phosphate, dibasic sodium phosphate and 1-octanol were purchased from Sigma-Aldrich (St. Louis, MO). Ethyl alcohol (200 proof) was bought from Decon Labs (King of Prussia, PA). Amoxicillin trihydrate and mercaptopurine monohydrate were acquired from Research Products International (Mount Prospect, IL). Beclomethasone dipropionate (BDP) was gifted from 3M (St. Paul, Minnesota). Acetic acid was bought from Fisher Scientific (Waltham, MA). Methanol was obtained from Spectrum Chemical Company (New Brunswick, NJ,). Acetonitrile was purchased from EMD (Gibbstown, NJ). Syringe filters (0.2 µm) were acquired from Pall Life Sciences (Port Washington, NY). Millipore water purification system with a 0.22µm filter was used for water.

5.3 Data collection

Aqueous solubilities were determined at room temperature for amoxicillin trihydrate, beclomethasone dipropionate (BDP) monohydrate, mercaptopurine monohydrate, and myricetin (MYR) monohydrate by conventional shake-flask methods and then analyzed by high performance liquid chromatography (HPLC). Dehydration and melting temperatures were acquired from differential scanning calorimetry (DSC) and water:drug stoichimentry was confirmed by thermogravimetric analysis (TGA). Log P values were gathered from the literature except in the case of myricetin monohydrate

which was determined experimentally. Aqueous solubility, dehydration and melting temperatures, and log P values for eleven additional compounds were also compiled. The entire sample set consisted of a variety of hydrate types (mono, di, tri) and included log P values ranging from -1.3 to 3.55.

5.4 Experimental

5.4.1 Differential scanning calorimetry (DSC)

Dehydration and melting analysis was performed via a Q1000 differential scanning calorimeter (DSC) with an auto sampler (TA Instruments, New Castle, DE) and calibrated with indium. Drug samples were weighed (3-4 mg) and placed into an aluminum hermetic pan with a pin-hole lid. The effect of DSC pan configuration was evaluated by comparing profiles of an aluminum hermetic pan, with and without a pin-hole lid, and a standard closed aluminum pan. No differences in thermal profiles were noted.

A nitrogen purge of 40 ml/min was used throughout. Samples were allowed to equilibrate at 30°C for five min, followed by a heat ramp of 10°C/min up to 50°C past the estimated melting point (T_M). Endotherms observed during the early stages of the thermal cycle were interpreted to represent solvent loss (water). The enthalpy of the phase

transition was calculated by the area under the curve for each endotherm while the entropy of the phase transition was obtained by the Equation 5.3.

$$\Delta S_x = \frac{\Delta H_x}{\Delta T_x} \quad \text{Eqn. 5.3}$$

Where:

ΔS_x Entropy of transition

ΔH_x Enthalpy of transition

ΔT_x Transition temperature (K)

5.4.2 Thermogravimetric analysis (TGA)

Confirmation of transition temperatures were conducted via thermogravimetric analysis (TGA), performed on a Q50 TGA (TA Instruments, New Castle, DE). Samples were weighed (3-4 mg) in open aluminum pans, and heated at 5°C/ min up to 50°C past the anticipated transition temperature. Weight loss as a function of temperature was analyzed and hydrate stoichiometry was estimated to confirm the expected water:drug relationship. A nitrogen purge of 60 ml/min was utilized throughout.

5.4.3 High performance liquid chromatography (HPLC)

Reverse-phase high performance liquid chromatography (HPLC) was used to analyze drug concentration from experimental conditions. Samples were analyzed with a Waters system consisting of an Alliance 2695 separation module, coupled with a 2487 dual absorbance detector (Waters Corporation, Milford, MA). Separation was achieved using a 150 mm x 3.9 mm Apollo C18 5.0 µm column. Isocratic methods were used throughout the investigations and drug concentrations were based on peak area.

5.4.3.1 Amoxicillin trihydrate

UV detection was conducted at 230 nm. A 96:4 mobile phase of potassium phosphate (pH 5):acetonitrile (ACN) with a run time of 8 min was utilized. Standards were prepared from roughly 1000 µg/ml stock solution of amoxicillin trihydrate in 100% methanol (MeOH) and ranged from 50-500 µg/ml. The retention time was approximately 3.5 min. Samples were run with a constant flow rate of 1.2 ml/min and an injection volume of 5 µl.

5.4.3.2 Beclomethasone dipropionate monohydrate

UV detection was conducted at 240 nm. A 70:30 mobile phase of ACN:H_2O with a run time of 10 min was utilized. Standards were prepared from roughly 200 µg/ml stock

solution of BDP monhydrate in a 90:10 ACN:H_2O solution and ranged from 10-100 µg/ml. The retention time for BDP monohydrate was approximately 7.5 min. Samples were run with a constant flow rate of 0.8 ml/min and an injection volume of 100 µl.

5.4.3.3 Mercaptopurine monohydrate

A 90:10 mobile phase MeOH:H_2O with a run time of 8 min was utilized. Standards were prepared from roughly 500 µg/ml stock solution of mercaptopurine monohydrate in 100% MeOH and ranged from 25-200 µg/ml. The retention time was approximately 3 min. Samples were run with a constant flow rate of 1.0 ml/min and an injection volume of 25 µl.

5.4.3.4 Myricetin monohydrate

See section 3.3.5

5.4.4 Partitioning Study

See section 3.3.7

5.4.5 Solubility Determination

Solubility values were determined (n=2) by adding excess drug to scintillation vials containing 20 ml of solvent and then agitated with a rocking shaker. Samples were collected at 30 and 60 min intervals for up to 8 hrs, and then again at 24 hrs. In an effort to improve solubility so that it could be determined within the limits of detection, 20% ethanol (EtOH) was utilized as a cosolvent during the investigation of BDP. Reverse phase high performance liquid chromatography (HPLC) was used to analyze drug concentration.

5.5 Results

5.5.1 Amoxicillin trihydrate

5.5.1.1 Differential scanning calorimetry (DSC)

The DSC curve for amoxicillin trihydrate can be seen in Figure 5.2.

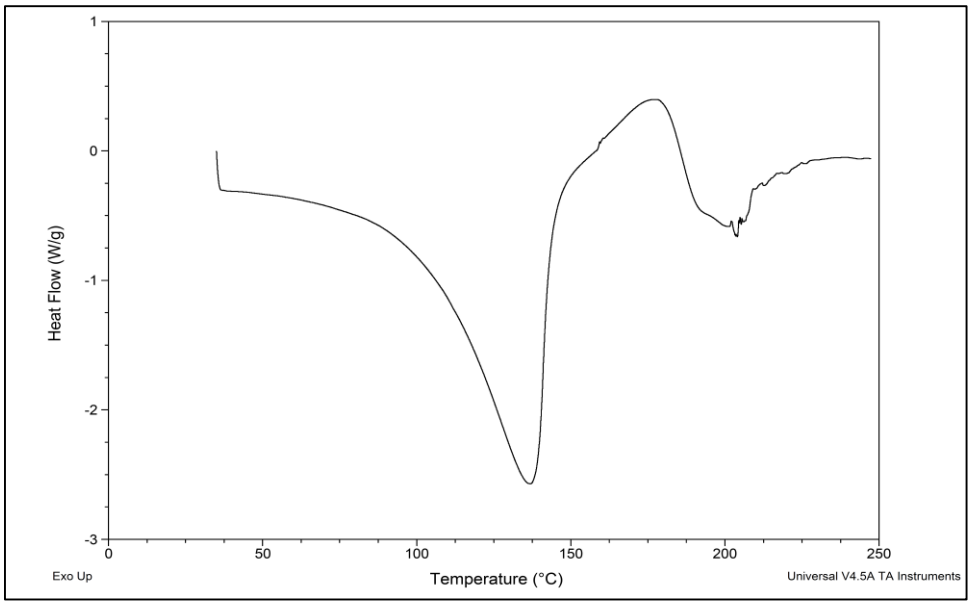

Figure 5.2 DSC profile of amoxicillin trihydrate.

The DSC profile for amoxicillin trihydrate exhibited a total of two endotherms (down). The second endotherm, onset temperature of 178°C, was deemed to be the melting point while the broad endotherm just prior, onset temperature of 104°C, is interpreted to represent solvent loss (water). The deep dehydration endotherm is a typical representation of drugs that have multiple water molecules attached to the drug molecule (Brittain, 2009). Entropies of the phase transitions were calculated from the endotherm onset and mid-point temperatures and can be seen in Table 5.1.

5.5.1.2 Thermogravimetric analysis (TGA)

TGA studies were performed on amoxicillin trihydrate and the profile can be seen in Figure 5.3. Weight loss as a function of temperature was analyzed to determine water

loss from the crystal. Weight loss attributed to dehydration was used to help determine the stoichiometry of water:drug molecules present.

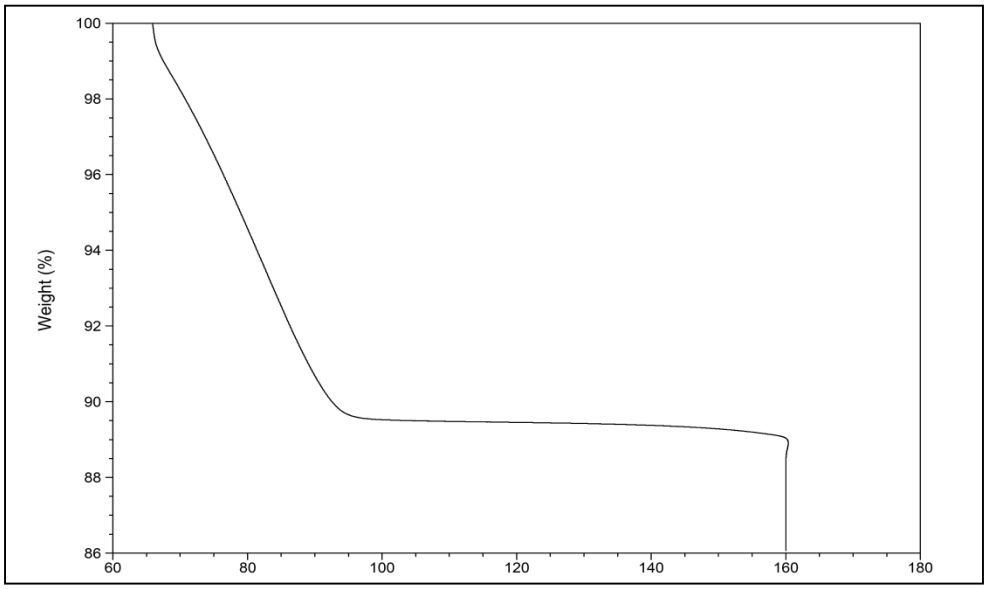

Figure 5.3 TGA profile of amoxicillin trihydrate.

The TGA for amoxicillin trihydrate showed a visible plateau with onset temperatures similar to its DSC profile (≈ 100°C). Weight loss attributed to dehydraion was estimated at 10.41% which calculates to roughly 3.34 moles of water per mole of amoxicillin.

5.5.1.3 Solubility determination

The average (n=2) dissolution profile for amoxicillin trihydrate can be seen in Figure 5.4. From the data, it can be determined that the initial solubility of amoxicillin

trihydrate was 2.87 mg/ml which remained relatively constant to 2.5 mg/ml for the first eight hours until reaching an average equilibrium value of 2.47 mg/ml after 24hrs.

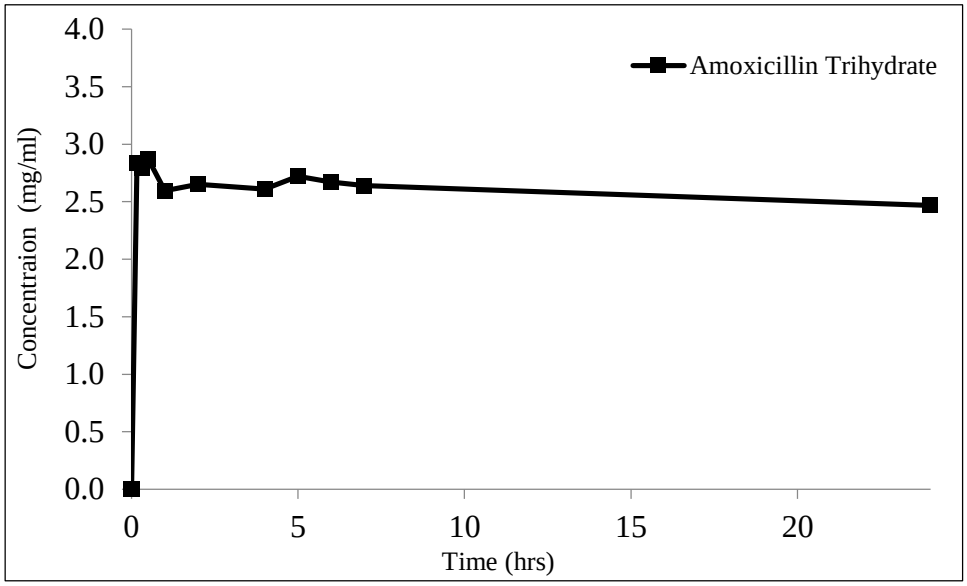

Figure 5.4 Dissolution profile of amoxicillin trihydrate.

5.5.2 Beclomethasone dipropionate monohydrate (BDP)

5.5.2.1 Differential scanning calorimetry (DSC)

BDP monohydrate was acquired by dissolving roughly 8mg/ml of the anhydrous crystal in a 95:5 EtOH:H_2O mixture that was then evaporated at room temperature. Crystals were collected and evaluated via DSC to confirm the presence of the monohydrate (Figure 5.5).

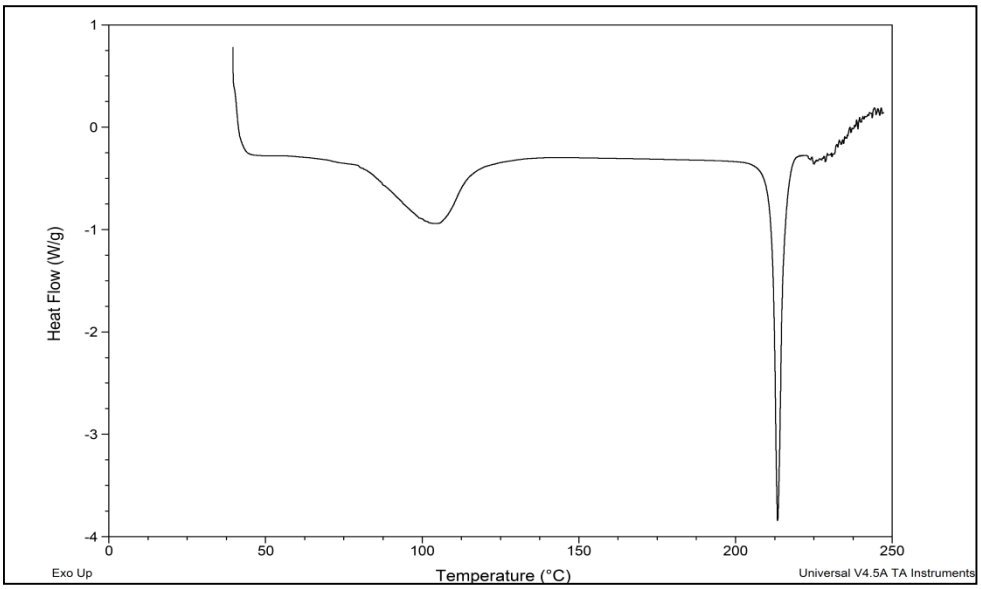

Figure 5.5 DSC profile of BDP monohydrate.

The DSC profile for BDP monohydrate exhibited a total of two endotherms (down). The second endotherm, onset temperature of 212°C, was deemed to be the melting point while the endotherm just prior to 100°C, onset temperature of 98°C, is interpreted to represent solvent loss (water). The sharp dehydration endotherm of BDP monohydrate is typical of hydrates that contain isolated binding sites (Brittain, 2009). Entropies of the phase transitions were calculated from the endotherm onset and mid-point temperatures and can be seen in Table 5.1.

5.5.2.2 Thermogravimetric analysis (TGA)

TGA studies were performed on BDP monohydrate and the profile can be seen in Figure 5.6. Weight loss as a function of temperature was analyzed to determine water loss

from the crystal. Weight loss attributed to dehydration was used to help determine the stoichiometry of water:drug molecules present.

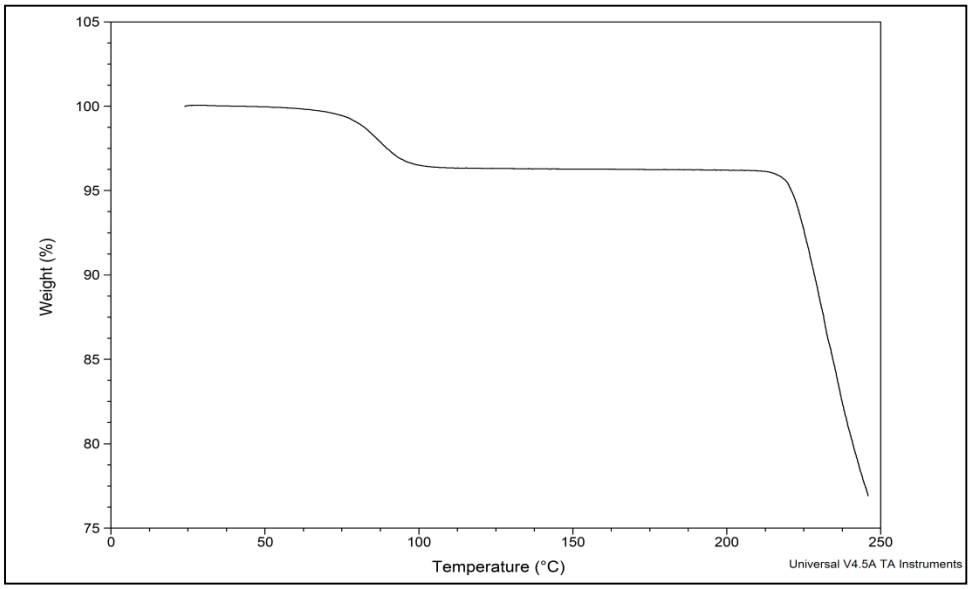

Figure 5.6 TGA profile of BDP monohydrate.

The TGA for BDP monohydrate showed a visible plateau with onset temperatures similar to its DSC profile (≈ 100°C). Total weight loss attributed to dehydration was estimated at 3.36% which calculates to roughly 1.01 moles of water per mole of BDP.

5.5.2.3 Solubility determination

The average (n=2) dissolution profile for BDP monhydrate can be seen in Figure 5.7. In an effort to improve solubility so that it could be determined within the limits of detection, 20% ethanol (EtOH) was utilized as a cosolvent. From the data, it can be seen

that the solubility of BDP monohydrate had a gradual increase over the eight hour time course, reaching an average equilibrium solubility of 3.09 µg/ml after 24 hrs.

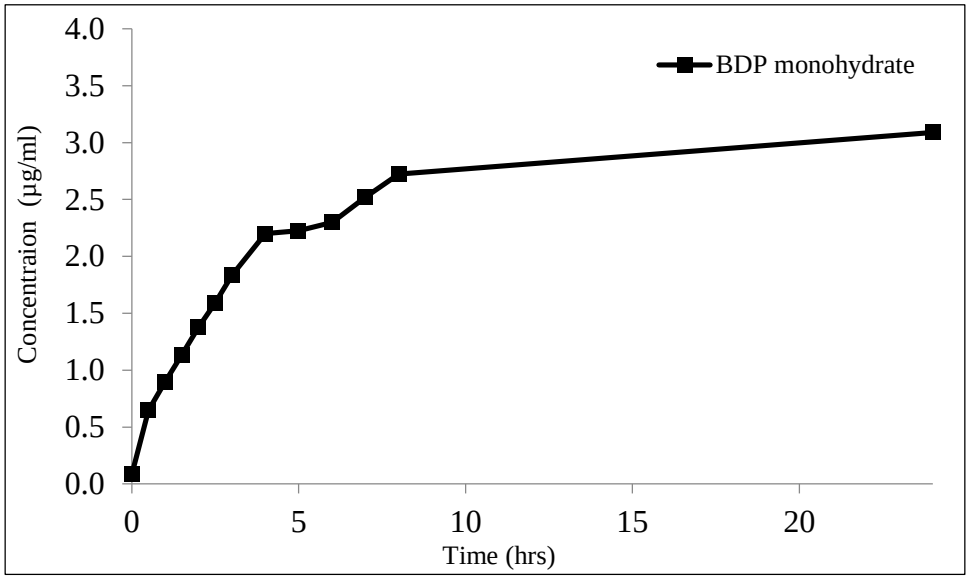

Figure 5.7 Dissolution profiles of BDP monohydrate.

5.5.3 Mercaptopurine monohydrate

5.5.3.1 Differential scanning calorimetry (DSC)

The DSC profile for mercaptopurine monohydrate (Figure 5.8) exhibited a total of two endotherms (down). The second endotherm, onset temperature of 316°C, was deemed to be the melting point while the endotherm just prior to 150°C, onset temperature of 142°C, is interpreted to represent solvent loss (water). The sharp dehydration endotherm of mercaptopurine monohydrate, along with the higher

dehydration temperature, is characteristic of hydrates that contain isolated binding sites (Brittain, 2009). Entropies of the phase transitions were calculated from the endotherm onset and mid-point temperatures and can be seen in Table 5.1.

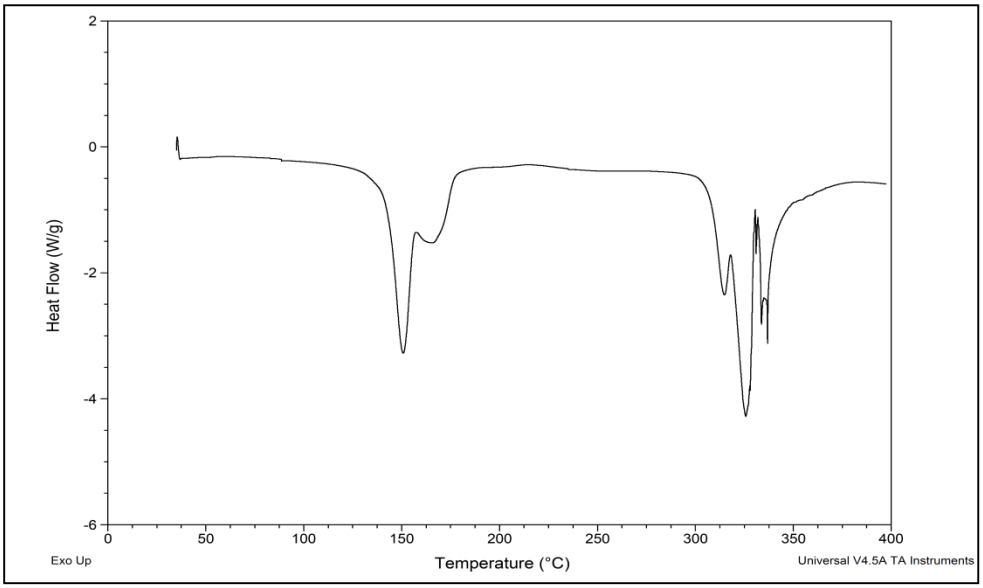

Figure 5.8 DSC profile of mercaptopurine monohydrate.

5.5.3.2 Thermogravimetric analysis (TGA)

TGA studies were performed on mercaptopurine monohydrate and the profile can be seen in Figure 5.9. Weight loss as a function of temperature was analyzed to determine water loss from the crystal. Weight loss attributed to dehydration was used to help determine the stoichiometry of water:drug molecules present.

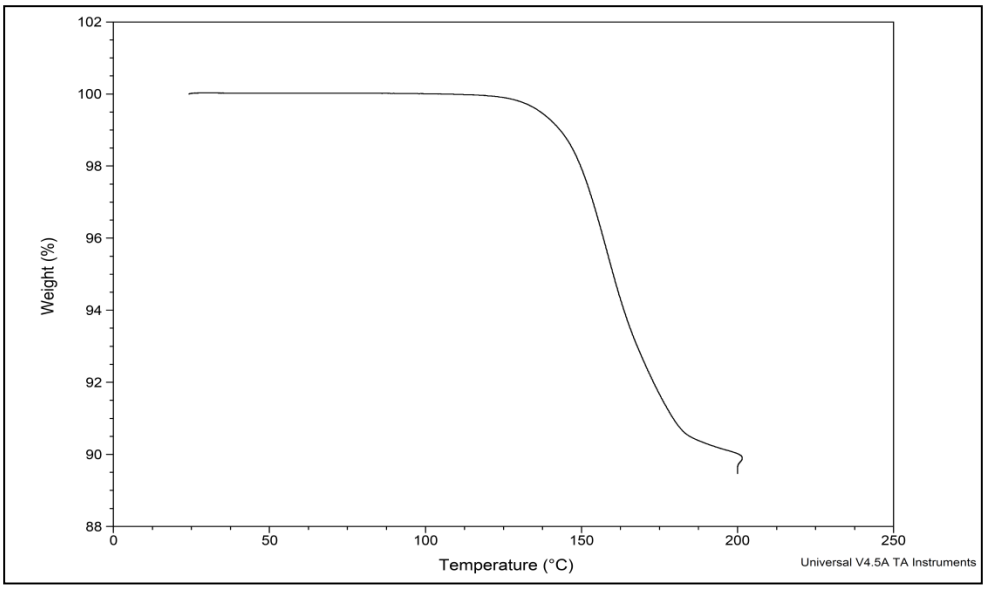

Figure 5.9 TGA profile of mercaptopurine monohydrate.

The TGA for mercaptopurine monohydrate showed a visible plateau with onset temperatures similar to its DSC profile (≈ 140°C). Total weight loss attributed to dehydration was estimated at 11.01% which calculates to roughly 0.93 moles of water per mole of mercaptopurine.

5.5.3.3 Solubility determination

The average (n=2) dissolution profile for mercaptopurine monhydrate can be seen in Figure 5.10. From the data, it can be determined that the solubility of mercaptopurine monohydrate had a gradual increase over the eight hour time course until reaching an average equilibrium solubility of 118.09 µg/ml after 24 hrs.

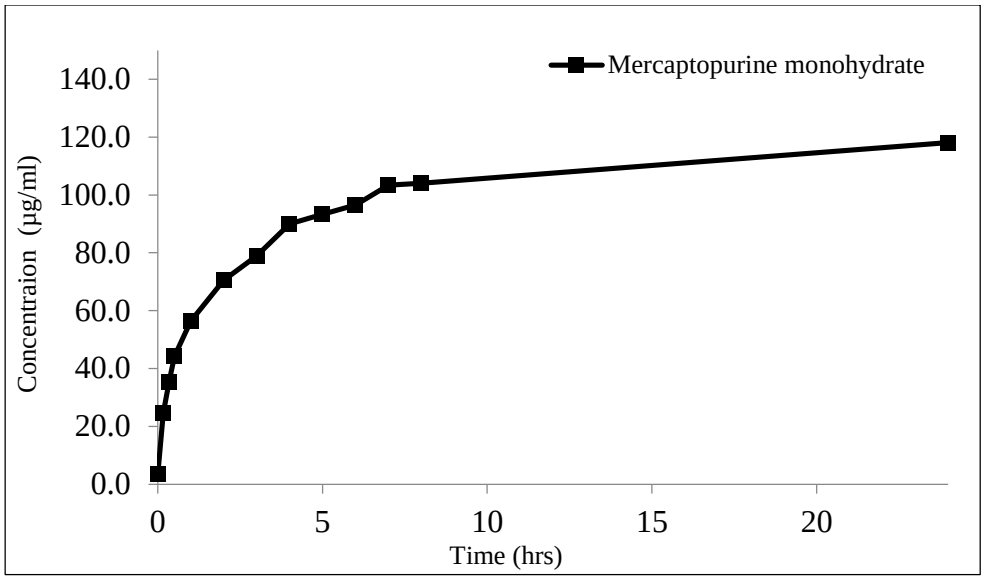

Figure 5.10 Dissolution profiles of mercaptopurine monohydrate.

5.5.4 Myricetin monohydrate

5.5.4.1 Differential scanning calorimetry (DSC)

See section 3.4.1

5.5.4.2 Thermogravimetric analysis (TGA)

See section 3.4.2

5.5.4.3 Solubility determination

See section 3.4.5

5.5.4.4 Partitioning Study

See section 3.4.6

5.5.5 Thermal Analysis Summary

Drug	**$T_{D\ (onset)}$ °C**	**ΔS_D cal/K*mol**	**$T_{M\ (onset)}$ °C**	**ΔS_M cal/K*mol**
Amoxicillin trihydrate	104	100.82	178	26.01
BDP monhydrate	98	30.07	212	17.73
Mercaptopurine monohydrate	142	28.15	316	16.49
Myricetin monohydrate	50	37.67	361	10.23

Table 5.1 Experimental data from thermal analysis.

5.5.6 Literature data

Aqueous solubility and thermal profiles of eleven drugs were collected from the literature. Experiments were conducted at room temperature and solubility values are presented as both μg/ml and mole fraction when comparing to predicted values generated from Equation 5.2. Both onset and midpoint dehydration temperatures were used for T_D and T_M and were gathered from DSC profiles in the literature. A summary of the literature data can be seen below in Table 5.2.

Drug (Log P)	Hydrate Type	Solubility (µg/ml)	Log Solubility (Mole Fraction)	T_D onset (°C)	T_M onset (°C)
Alprazolam[1,2] (2.23)	Di	100	-5.28	68	226
Ampicillin[3,4] (1.35)	Tri	7850	-3.46	80	205
Caffeine[5] (-0.07)	0.8	22000	-2.72	58	235
Carbamazepine[6,7] (2.45)	Di	125	-5.08	60	185
Doxycycline[8,9] (-0.02)	Mono	1800	-4.15	155	205
Fluconazole[10] (0.50)	Mono	3560	-3.70	98	132
Lamivudine[11] (-1.30)	0.2	84900	-2.19	135	160
Phenobarbital[12] (1.47)	Mono	1209	-4.06	55	174
Piroxicam[13,14] (1.68)	Mono	12.4	-6.19	158	198
Stavudine[15] (-0.80)	0.33	90600	-2.15	142	171
Theophylline[16,17] (-0.17)	Mono	6737	-3.21	71	271

Table 5.2 Literature data summary.

1 (Laihanen, 1996)
2 (Caira, 1994)
3 (Zhu, 1996)
4 (Liu, 2004)
5 (Edwards, 1997)
6 (Murphy, 2002)
7 (Katzhendler, 1998)
8 (Legendre, 2012)
9 (Honary, 2012)
10 (Alkhamis, 2002)
11 (Jozwiakowski, 1995)
12 (Sekiguchi, 1973)
13 (Qu, 2011)
14 (Vrečer, 2003)
15 (Gandhi, 1999)
16 (Grant, 1994)
17 (Suzuki, 1989)

5.6 Results

5.6.1 Prediction with onset temperatures

Literature data were combined with values that were produced in the laboratory and plotted as predicted versus experimental mole fraction solubility for each hydrate (Figure 5.11). Recall Equation 5.2, where ΔS_M is estimated by 13.5 cal/K*mol, and ΔS_D is approximated by 26 cal/K*mol. Initially, onset temperatures were used for the dehydration temperature (T_D) and the melting point (T_M).

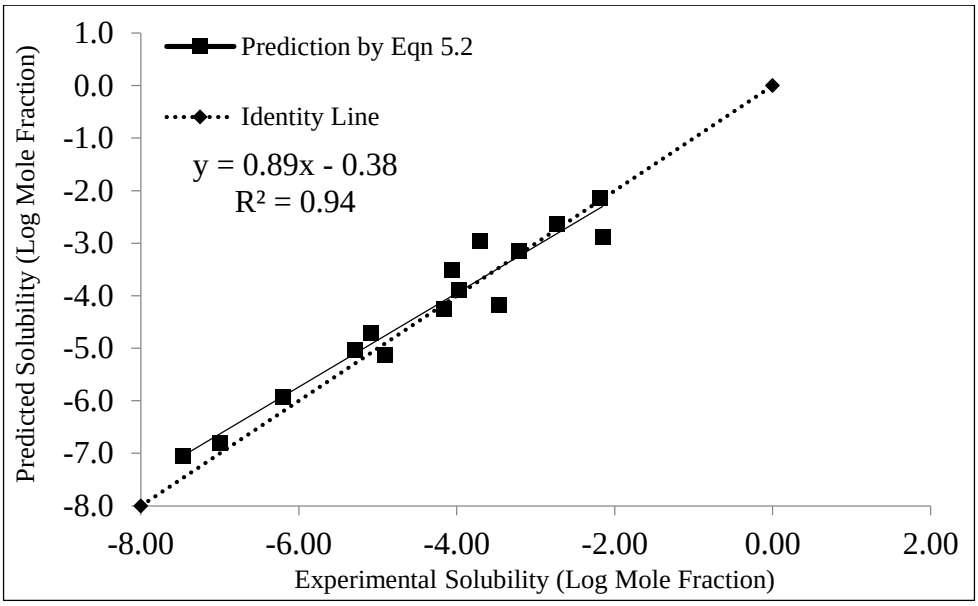

Figure 5.11 Predicted vs. experimental solubility using onset transition temperatures.

In this version of the model the data suggest a strong correlation between predicted solubility and experimental data that was generated in the laboratory and acquired from the literature. By accounting for both dehydration and melting, using the onset temperature for both phase transitions, the model resulted in an R^2=0.94 and an average absolute error of 0.30 log units.

5.6.2 Prediction with midpoint temperatures

To gain an appreciation for the variability that can occur when estimating solubility in this manner, the same data set was analyzed using endotherm midpoint temperatures for both dehydration and melting (Figure 5.12).

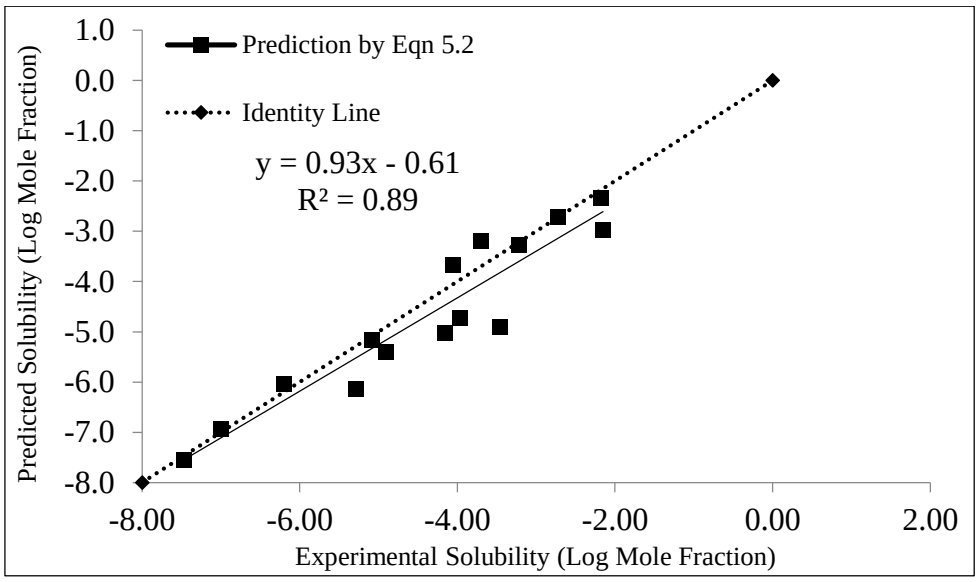

Figure 5.12 Predicted vs. experimental solubility using midpoint transition temperatures.

The data from Figure 5.12 indicates there is a noticeable correlation between predicted solubility and experimental data when using midpoint transition temperatures, however, it appears to be less significant when compared to the correlation seen in Figure 5.11. While the slope of this relationship is 0.93, providing a closer observed value to the ideal value of 1.0, the slope falls noticeably below the identity line as solubility increases. Estimating the hydrate solubility by accounting for both dehydration and melting, while using the midpoint temperature for both transitions, resulted in an R^2=0.89 and an average absolute error of 0.46 log units.

5.6.3 Prediction with constant dehydration temperature

To further the practicality of this model, solubility estimations were also conducted using a constant dehydration temperature of 100°C, should dehydration temperature be unattainable (Figure 5.13). Onset temperature was once again used for $T_{M.}$

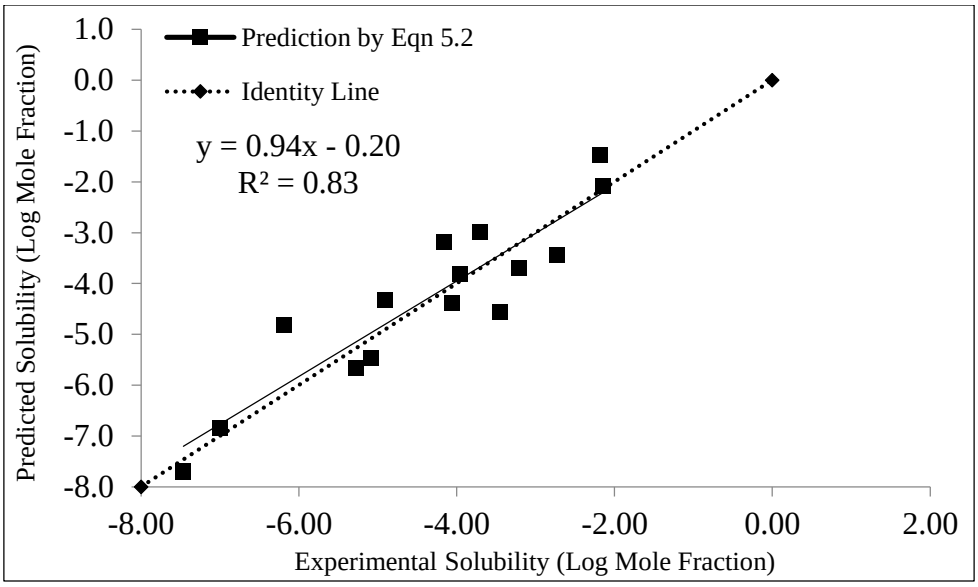

Figure 5.13 Predicted vs. experimental solubility using a constant dehydration temperature (100°C) and onset melting temperatures.

The data from Figure 5.13 indicate that there is a reasonable correlation between predicted solubility and experimental data when using a constant dehydration temperature of 100°C and the onset melting temperatures, however, there is less correlation with the data set when compared to the estimation seen in Figure 5.11. Interestingly, the slope of this relationship is 0.94, providing a closer observed value to the ideal value of 1.0 but there is noticeably more scatter amongst the data points. Estimating hydrate solubility by accounting for both dehydration and melting, while using an approximation for dehydration (100°C) and the onset temperature for melting, resulted in an R^2=0.83 and an average absolute error of 0.56 log units.

5.6.4 Prediction comparison to the GSE

The solubility of the data set was estimated by the general solubility equation (Equation 4.7) giving log molar solubility. A comparison of relative error (predicted-experimental) of the log solubility (µg/ml) between the two equations can be seen in Figure 5.14.

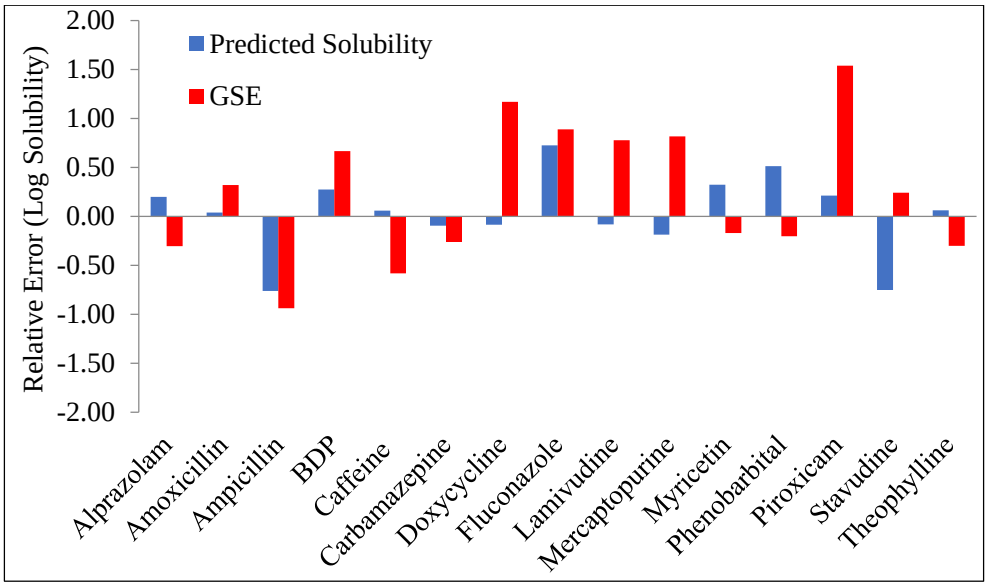

Figure 5.14 Relative error of the log solubility (µg/ml) for each estimation.

The data in Figure 5.14 compares the relative error for solubility estimation of a hydrate, using both the hydrate prediction equation (Equation 5.2) and the GSE (Equation 4.7). The data suggest that the usefulness of the hydrate prediction equation is relatively significant, as it has less relative error throughout the data set when compared to the GSE. However, it is important to remember that the GSE, like most solubility estimation

models, is designed specifically for an anhydrous crystal. This comparison is merely used to illustrate the need for a solubility prediction model for hydrates as they are an essential aspect to the pharmaceutical field.

5.6.5 Summary

A summary of experimental solubility, predicted solubility using onset transition temperatures, and absolute error for each compound can be seen in Table 5.3.

Drug (Log P)	Hydrate Type	Experimental Log Solubility (µg/ml)	Predicted Log Solubility (µg/ml)	Log Absolute Error
Alprazolam (2.23)	Di	2.00	2.20	0.20
Amoxicillin (0.87)	Tri	3.39	3.43	0.04
Ampicillin (1.35)	Tri	3.89	3.13	0.76
BDP (3.55)	Mono	0.48	0.62	0.14
Caffeine (-0.07)	0.8	4.34	4.40	0.06
Carbamazepine (2.45)	Di	2.10	2.44	0.34
Doxycycline (-0.02)	Mono	3.26	3.13	0.12
Fluconazole (0.50)	Mono	3.55	4.28	0.73
Lamivudine (-1.30)	0.2	4.93	4.96	0.03
Mercaptopurine (0.01)	Mono	2.07	1.81	0.25
Myricetin (2.94)	Mono	-0.19	0.16	0.35
Phenobarbital (1.47)	Mono	3.08	3.60	0.51
Piroxicam (1.68)	Mono	1.09	1.31	0.21
Stavudine (-0.80)	0.33	4.96	4.21	0.75
Theophylline (-0.17)	Mono	3.83	3.87	0.04
Average				**0.30**

Table 5.3 Summary of experimental solubility, predicted solubility, and absolute error.

The solubility data in Table 5.3 are presented in log µg/ml as it is a more functional metric when discussing solubility compared to log mole fraction. No

discernible patterns can be determined from the data set with regard to a relationship between absolute error, log P or hydrate type. In fact, the three drugs with the greatest absolute error include a mono, tri, and 0.33 hydrate with corresponding log P values of 0.5, 1.35, and -0.8 covering a wide range of the analyzed data.

5.7 Conclusion

The estimation of solubility for a drug or drug candidate is an important aspect to the drug development process for both academic and industrial research. The hydrate of a drug substance usually has a lower aqueous solubility compared to its anhydrous form. Current estimation models tend to only consider the anhydrous crystal, and don't account for additional energetics that may be present. This can lead to an over-prediction for hydrate solubility which can lead to unexpected results, including poor or unpredictable product performance. By improving the accuracy of solubility estimation, drug development studies involving hydrates can be designed accordingly.

Data suggest a strong correlation between predicted solubility and experimental data that was acquired both in the laboratory and from the literature. The data set includes compounds with different hydrate types and log P values that vary from -1.3 to 3.55. Most notably, experimental solubility's (log μg/ml) ranged as low as -0.19 and as high as 4.96. The average absolute error for the entire data set is 0.30 log units providing a good indication of the overall usefulness of the model presented.

REFERENCES

Ademola, J., (1997) Transdermal and Topical Drug Delivery. 1st edition; Interpharm Press, Inc., Buffalo Grove, IL, pp 511-513.

Alkhamis, K.A., Obaidat, A.A., Nuseirat, A.F., (2002) Solid-State Characterization of Fluconazole. Pharm. Dev. Technol. 7: 491-503.

Bachelor, M.A., Cooper, S.J., Sikorski, E.T., Bowden, G.T., (2005) Inhibition of p38 mitogen-activated protein kinase and phosphatidylinositol 3-kinase decreases UVB-induced activator protein-1 and cyclooxygenase-2 in a SKH-1 hairless mouse model. Mol. Cancer Res. 3: 90-99.

Barry, B.W., (1993) Dermatological Formulations. Percutaneous Absorption. Marcel Dekker, Inc., New York, NY, pp 145-159.

Barthelman, M., Chen, W., Gensler, H.L., Huang, C., Dong, Z., Bowden, G.T., (1998) Inhibitory effects of perillyl alcohol on UVB-induced murine skin cancer and AP-1 transactivation. Cancer Res. 58: 711-716.

Biniek, K., Levim K., Dauskardt, R.H., (2012) Solar UV radiation reduces the barrier function of human skin. PNAS. 42: 17111-17116.

Brittain, H.G., Morris, K.R., (2009) Polymorphism in Pharmaceutical Solids. 2nd edition; Informa Healthcare, Inc., New York, NY, pp 233-281.

Chen, W., Borchers, A.H., Dong, Z., Powell, M.B., Bowden., G.T., (1998) UVB irradiation-induced activator protein-1 activation correlates with increased c-fos gene expression in a human keratinocyte cell line. J. Biol. Chem. 273: 32176-32181.

Chen-Yu, G., Chun-fen, Y., Qi-lu, L., Qi, T., (2012) Development of a Quercetin-loaded nanostructured lipid carrier formulation for topical delivery. Int. J. Pharm. 430: 292-298.

Caira, M.R., Easter, B., Honiball, S., Horne, A., Nassimbeni, L.R., (1994) Structure and thermal stability of Alprazolam and selected solvates. J. Pharm. Sci. 84: 1379-1384.

Cooper, S. J., MacGowan, J., Ranger-Moore, J., Young, M.R., Colburn, N.H., Bowden, G.T., (2003) Expression of dominant negative c-jun inhibits ultraviolet B-induced squamous cell carcinoma number and size in an SKH-1 hairless mouse model. Mol. Cancer Res. 11: 848-54.

Dang, Y., Lin, G., Xie, Y., Duan, J., (2013) Quantitative determination of myricetin in rat plasma by ultra performance liquid chromatography tandem mass spectrometry and its absolute bioavailability. Drug Res. 64: 516-522.

Dickinson, S.E., Melton, T.F., Olson, E.R., Zhang, J., Saboda, K., Bowden, G.T., (2009) Inhibition of activator protein-1 by sulforaphane involves interaction with cysteine in the cFos DNA-binding domain: implications for chemoprevention of UVB-induced skin cancer. Cancer Res. 69: 7103-7110.

Diepgen, T.L., Mahler, V., (2002) The epidemiology of the skin. Br. J. Dermatol. 61: 1-6.

Dinkova-Kostova, A.T., Jenkins, S.N., Fahey, J.W., Ye, L., Wehage, S.L., Liby, K.T., Stephenson, K.K., Wade, K.L., Talalay, P., (2006) Protection against UV-light-induced skin carcinogenesis in SKH-1 high-risk mice by sulforaphane-containing broccoli sprout extracts. Cancer Lett. 240: 243-252.

Dinkova-Kostova, A.T., Fahey, J.W., Wade, K.L., Jenkins, S.N., Shapiro, T.A., Fuchs, E.J., Kerns, M.L., Talalay, P., (2007) Induction of the phase 2 response in mouse and human skin by sulforaphane-containing broccoli sprout extracts. Cancer Epidemiol. Biomarkers Prev. 16: 847-851.

Edwards, H.G.M., Lawson, E., de Matas, M., Shields, L., York, P., (1997) Metamorphosis of caffeine hydrate and anhydrous caffeine. J. Chem. Soc. Perkin Trans 2. 1: 1985-1990.

Faller, B., Ertl, P., (2007) Computational approaches to determine drug solubility.Adv. Drug Deliv. Rev. 59: 533-545.

Gandhi, R.B., Bogardus, J.B., Bugay, D.E., Perrone, M.A., Kaplan, M.A., (2000) Characterization of piroxicam crystal modifications. Int. J. Pharm. 201: 221-237.

Ghosh, T.K., (1997) Transdermal and Topical Drug Delivery Systems. Interpharm Press, Inc., Buffalo Grove, IL, pp 1-32.

Gilchrest, B.A., Eller, M.S., Geller, A.C., (1999) The pathogenesis of melanoma induced by ultraviolet radiation. N. Engl. J. Med. 340: 1341-1348.

Glanz, K., Buller, D.B., Saraiya, M., (2007) Reducing ultraviolet radiation exposure among outdoor workers: state of the evidence and recommendations. Environ. Health. 6: 22.

Gosh, T.K., Pfister, W., (1997) Transdermal and Topical Drug Delivery. 1st edition; Interpharm Press, Inc., Buffalo Grove, IL, pp 3-8.

Grant, D., Khankari, R.K., (1995) Pharmaceutical hydrates. Thermochim. Acta. 248: 61-79.

Gupta, A., Myrdal, P.B., (2004) Development of a perillyl alcohol topical cream formulation. Int. J. Pharm. 269: 373-383.

Hakkinen, S.H., Karenlampi, S.O., Heinonen, I.M., Mykkanenm H.M., Torronen, A.R., (1999) Content of the flavonols quercetin, myricetin, and kaempferol in 25 edible berries. J. Agric. Food Chem. 47: 2274-2249.

Hertog, M.G.L., Fresken, E.J.M., Hollman, P.C.H., (1993) Dietary antioxidative flavonoids and risk of coronary heart disease: the Zutphen Elderly Study. Lancet. 342: 1007-1011.

Hoelgaard, A., Moller, N., (1983) Hydrate formation of metronidazole benzoate in aqueous suspensions. Int. J. Pharm.15: 213-221.

Holbrook, K.A., (1993) The Structure and Development of Skin. Dermatology in General Medicine. 4th edition; McGraw Hill, Inc., New York, NY, pp 97-145.

Honary, S., Zahir, F., (2012) Effect of process factors on the properties of doxycycline nanovesicles. Trop. J. Pharm. Res. 11: 169-175.

Hong, C., Xie, Y., Yao, Y., Li, G., (2014) A novel strategy for Pharmaceutical cocrystal generation without knowledge of stoichiometric ratio: Myricetin cocrystals and a ternary phase diagram. Pharm. Res. DOI: 10.1007/s11095-014-1443-y.

Jain, N., Yalkowsky, S.H., (2001) Estimation of the Aqueous Solubility I: Application to Organic Nonelectrolytes. J. Pharm. Sci. 90: 234-252.

Jin, Y., Wang, M., Rosen, R.T., Ho, C.T., (1999) Thermal Degradation of Sulforaphane in Aqueous Solution. J. Agric. Food Chem. 47: 3121-3123.

Jozwiakowski, M.J., Nguyen, N.T., Sisco, J.M., Spancake, C.W., (1996) Solubility behavior of Lamivudine Crystal Forms in Recrystallization Solvents. J. Pharm. Sci. 85: 193-199.

Juge, N., Mithen, R.F., Traka, M., (2007) Molecular basis for chemoprevention by sulforaphane: a comprehensive review. Cell Mol. Life Sci. 64: 1105-1127.

Jung, S.K., Lee, K.W., Byun, S., (2008) Myricetin suppresses UVB-induced skin cancer by targeting Fyn. Cancer Res. 68: 6021-6029.

Karagas, M.R., Stannard, V.A., Mott, L.A., (2002) Use of tanning devices and risk of basal and squamous cell skin cancers. J. Natl. Cancer Inst. 94: 224-226.

Katzhendler, I., Azoury, R., Friedman, M., (1998) Crystalline properties of carbamazepine in sustained release hydrophilic matrix tablets based on hydroxypropyl methylcellulose. J. Controlled Release. 1: 69-85.

Kirchhoff, G., (1860) On the relation between the radiating and absorbing powers of different bodies for light and heat (Translated by Guthrie, F of Philosophical Magazine). Annalen der Physik.109: 275-301.

Laihanen, N., Muttonen, E., Laaksonen, M., (1996) Solubility and intrinsic dissolution rate of Alprazolam crystal modifications. Pharm. Dev. Technol. 1: 373-380.

Lampe, M.A., (1983) Human Stratum Corneum Lipids: Characterization and Regional Variations. J. Lipid Res. 24: 120-130.

Lauro, M.R., Torre, M.L., Maggi, L., De Simone, F., Conte, U., Aquino, R.P., (2002) Fast-and slow-release tablets for oral administration of flavonoids: rutin and quercetin. Drug Dev. Ind. Pharm. 28: 371-379.

Lee, K.W., Kang, N.J., Rogozin, E.A., (2007) Myricetin is a novel natural inhibitor of neoplastic cell transformation and MEK1. Carcinogenesis. 28: 1918-1927.

Legendre, A.O., Silva, L.R.R., Silva, D.M., Rosa, I.M.L., (2012) Solid state chemistry of the antibiotic doxycycline: structure of the neutral monohydrate and insights into its poor water solubility. Cryst. Eng. Comm. 14: 2532-2540.

Li, J.J., Dong, Z., Dawson, M.I., Colburn, N.N., (1996) Inhibition of tumor promoter-induced transformation by retinoids that transrepress AP-1 without transactivating retinoic acid response element. Cancer Res. 56: 483-489.

Li, Y., Ding, Y., (2013) Therapeutic potential of myricetin in diabetes mellitus. Food Science and Human Wellness. 1: 19-25.

Liu, C.L., Wu, S.M., Chang, T.C., (2004) Analysis of a mixture containing ampicillin anhydrate and ampicillin trihydrate by thermogravimetry, oven heating, differential scanning calorimetry, and X-ray diffraction techniques. Anal. Chim. Acta. 517: 237-243.

Lucas-Abellán, C., Fortea, I., Gabaldón, J.A., (2008) Encapsulation of quercetin and myricetin in cyclodextrins at acidic pH. J. Agric. Food Chem. 56: 255-259.

Mao, C., Pinal, R., Morris, K.R., (2005) A Quantitative Model to Evaluate Solubility Relationship of Polymorphs from Their Thermal Properties. Pharm. Res. 22: 1149-1157.

Meeran, S.M., Punathil, T., Katiyar, S.K., (2008) Interleukin-I2-deficiency exacerbates inflammatory responses in UV-irradiated skin and skin tumors. J. Invest. Dermatol. 128: 2716-2727.

Melnikova, V.O., Ananthaswamy, H.N., (2005) Cellular and molecular events leading to the development of skin cancer. Mutat. Res. 571: 91-106.

Murphy, D., Rodriguez,-Cintron, F., Langevin, B., Kelly, R.C., Rodriguez-Hornedo, N., (2002) Solution-mediated phase transformation of anhydrous to dehydrate carbamazepine and the effect of the lattice disorder. Int. J. Pharm. 246: 121-134.

Narayanan, D.L., Saladi, R.N., Fox, J.L., (2010) Ultraviolet radiation and skin cancer. Int. J. Dermatol. 49: 978-986.

Neau, S.H., Flynn, G.L., (1990) Solid and liquid heat capacities of n-Alkyl Para-aminobenzoates Near the Melting Point. Pharm. Res. 7: 1157-1162.

Petermann, K.B., Rozenberg, G.I., Zedek, D., (2007) CD200 is induced by ERK and is a potential therapeutic target in melanoma. J. Clin. Invest. 117: 3922-3929.

Poole, J.W., Owen, G., Silverio, J., Freyhof, J.N., Rosenman, S.B., (1968) Physiochemical factors influencing the absorption of the anhydrous and trihydrate forms of ampicillin. Curr. Thera. Res.10: 292-303.

Preston, D.S., Stern, R.S., (1992) Nonmelanoma cancers of the skin. N. Engl. J. Med. 327: 1649-1662.

Pudipeddi, M., Serajuddin, A.T.M., (2005) Trends in Solubility of Polymorphs. J. Pharm. Sci. 94: 929-939.

Qu, H., Munk, T., Cornett, C., (2011) Influence of Temperature on Solvent-Meditated Anhydrate-to- Hydrate Transformation Kinetics. Pharm. Res. 28: 364-373.

Rodriguez-Hornedo, N., Lechuga-Ballesteros, D.,Wu, H. J., (1992) Phase transition and heterogeneous/epitaxial nucleation of hydrated and anhydrous theophylline crystals. Int. J. Pharm. 85: 149-162.

Ribeiro de Lima, M.T., Waffo-Teguo, P., Teissedre, P.L., (1999) Determination of stilbenes (trans-astringin, cis and trans-piceid, and cis amd trans-resveratrol) in Portuguese wines. J. Agric. Food Chem. 47: 2666-2670.

Rincon, M., Flavell, R.A., (1994) AP-1 transcriptional activity requires both T-cell receptor-mediated and co-stimulatory signals in primary T lymphocytes. Embo. J. 13: 4370-4381.

Rittié, L., Kansra, S., Stroll, S.W., (2007) Differential ErbBI signaling in squamous cell versus basal cell carcinoma of the skin. Am. J. Pathol. 170: 2089-2099.

Sekiguchi, K., Kanke, M., Tsuda, Y., Ishida, K., Tsuda, Y., (1973) Dissolution Behavior of Solid Drugs III: Determination of the Transition Temperature between the Hydrate and Anhydroys'Forms of Phenobarbital by Measuring Their Dissolution Rates. Chem. Pharm. Bull. 21: 1592-1600.

Setlow, R.B., (1974) The wavelengths in sunlight effective in producing skin cancer: a theoretical analysis. Proc. Natl. Acad. Sci. 71: 3363-3366.

Siegel, R., Ma, J.M., Zou, Z., Jemal, A., (2014) Cancer Statistics 2014. CA. 64: 9-29.

Sowa, M., Ślepokura, K., Matczak-Jon, E., (2014) A 1:1 pharmaceutical cocrysral myricetin in combination with uncommon piracetam conformer: X-Ray single crystal analysis and mechanochemical synthesis. J. Mol. Struct. 1058: 114-121.

Stephenson, G.A., Groleau, E.G., Kleeman, R.L., (1998) Formation of isomorphic desolvates: creating a molecular vaccum. J. Pharm. Sci. 87: 536-542.

Suárez, B., López-Abente, G., Martínez, C., (2007) Occupation and skin cancer: the results of the HELIOS-I multicenter case-control study. BMC Public Health. 7: 180.

Suh, Y.J., (2003) Cancer chemoprevention with dietary phytochemicals. Nat. Rev. 3: 768-780.

Suzuki, E., Shimomura, K., Sekiguchi, K., (1989) Thermochemical Study of Theophylline and Its Hydrate. Chem. Pharm. Bull. 37: 493-497.

Talalay, P., Fahey, J.W., Healy, Z.R., Wehage, S.L., Benedict, A.L., Min, C., Dinkova-Kostova, A.T., (2007) Sulforaphane mobilizes cellular defenses that protect skin against damage by UV radiation. Proc. Natl. Acad. Sci. U S A. 104: 17500-17505.

Vrečer, F., Vrbic, M., Meden, A., (2003) Characterization of piroxicam crystal modifications. Int. J. Pharm. 256: 3-15.

Walden, P., (1908) Über die Schmelzwärme, spezifische Kohäsion und Molekulargrösse bei der Schmelztemperatur. Zeitschrift für Elektrochemie und angewandte physikalische Chemie, 14: 713-724.

Wang, S., Ye., T., Zhang, X., Yang, R., Yi, X., (2013) Myricetin microemulsion for oral drug delivery: formulation optimization, in situ intestinal absorption and in-vivo evaluation. AJPS. 8: 18-27.

Xiao, Q., Liang., H., Yuan, Q., (2009) Effect of Temperature, pH and Light on the Stability of Sulforaphane Solution. Chin. Pharm. J. 43: 193-196.

Yalkowsky, S.H., Mishra, D.S., (1992) Ideal Solubility of a Solid Solute: Effect of Heat Capacity Assumptions. Pharm. Res. 9: 958-959.

Yao, Y., Lin, G., Xie, Y., Ma, P., (2014) Preformultation studies of myricetin: a natural antioxidant flavonoid. Pharmazie. 69: 19-26.

Young, W.W.L., Suryanarayanan, R., (1991) Kinetics of transition of anhydrous carbamazepine to carbamazepine dehydrate in aqueous suspensions. J. Pharm Sci. 80: 496-500.

Zhu, Haijian., Grant, D., (1996) Influence of water activity in organic + water mixtures on the nature of the crystallizing drug phase. 2. Ampicillin. Int. J. Pharm. 139: 33-43.